RESEARCH ARTICLE

Novel insight into the role of clusterin on intraocular pressure regulation by modifying actin polymerization and extracellular matrix remodeling in the trabecular meshwork

Avinash Soundararajan[1] | Ting Wang[1,2] | Sachin A. Ghag[1] | Min H. Kang[3] |
Padmanabhan P. Pattabiraman[1,2]

[1]Department of Ophthalmology, Glick Eye Institute, Indiana University School of Medicine, Indianapolis, Indiana, USA

[2]Stark Neuroscience Research Institute, Indiana University Purdue University Indianapolis, Indianapolis, Indiana, USA

[3]Department of Ophthalmology and Visual Sciences, University Hospitals Eye Institute, Case Western Reserve University School of Medicine, Cleveland, Ohio, USA

Correspondence
Padmanabhan Paranji Pattabiraman, Glick Eye Institute, Department of Ophthalmology, Indiana University School of Medicine, 1160 West Michigan St, Indianapolis, IN, USA.
Email: ppattabi@iu.edu

Abstract

This study provides comprehensive mechanistic evidence for the role of clusterin, a stress-response secretory chaperone protein, in the modulation of intraocular pressure (IOP) by regulating the trabecular meshwork (TM) actin cytoskeleton and the extracellular matrix (ECM). The pathological stressors on TM known to elevate IOP significantly lowered clusterin protein levels indicating stress-related clusterin function loss. Small interfering RNA-mediated clusterin loss in human TM cells in vitro induced actin polymerization and stabilization via protein kinase D1, serine/threonine-protein kinase N2 (PRK2), and LIM kinase 1 (LIMK1), and the recruitment and activation of adhesome proteins including paxillin, vinculin, and integrin αV and β5. A complete loss of clusterin as seen in clusterin knockout mice ($Clu^{-/-}$) led to significant IOP elevation at postnatal Day 70. Contrarily, constitutive clusterin expression using adenovirus (AdCLU) in HTM cells resulted in the loss of actin polymerization via decreased PRK2, and LIMK1 and negative regulation of integrin αV and β5. Furthermore, we found that AdCLU treatment in HTM cells significantly decreased the ECM protein expression and distribution by significantly increasing matrix metalloprotease 2 (MMP2) activity and lowering the levels of pro-fibrotic proteins such as transforming growth factor-β2 (TGFβ2), thrombospondin-1 (TSP-1), and plasminogen activator inhibitor-1 (PAI-1). Finally, we found that HTM cells supplemented with recombinant human clusterin attenuated the pro-fibrotic effects of TGFβ2. For the first time this study demonstrates the importance of clusterin in the regulation of TM actin cytoskeleton - ECM interactions and the maintenance of IOP, thus making clusterin an interesting target to reverse elevated IOP.

KEYWORDS
actin cytoskeleton, clusterin, extracellular matrix, fibrosis, intraocular pressure, trabecular meshwork

1 | INTRODUCTION

The trabecular meshwork (TM) along with juxtacanalicular tissue (JCT) and the Schlemm's Canal (SC) of the human conventional aqueous humor (AH) outflow pathway aids in 60%–80% of aqueous humor (AH) drainage (Goel et al., 2010). The TM tissue is a series of collagenous fenestrated beams lined by the TM cells. The intraocular pressure (IOP) is generated from the resistance offered to the AH drainage by the outflow pathway tissue in the JCT region of the TM and the inner wall of SC. Normal AH drainage results from a fully functional TM outflow pathway. The TM tissue is constantly subjected to various physiological stress including—oxidative stress, endoplasmic reticulum stress, protein misfolding, and accumulation of excessive proteinaceous materials—during development and normal aging (Pattabiraman & Toris, 2016). Under physiological conditions, cellular stress response systems including antioxidants, chaperones, and heat shock proteins come in aid as tissue repair machinery (Kourtis & Tavernarakis, 2011). Aging and cellular senescence can cause a failure to activate such cellular repair signals leading to pathological endpoints including improper AH drainage, and elevated IOP. Various protein and lipid growth factors are present in the glaucomatous AH over the threshold levels including—transforming growth factor β2 (TGFβ2), connective tissue growth factor (CTGF), lysophosphatidic acid, and sphingosine-1-phosphate (S1P) and are known to cause IOP elevation (Liu et al., 2018). Elevated IOP stress by itself can trigger a feed-forward activation loop towards accelerating IOP elevation by increasing Rho GTPase signaling and inducing contractile activity in TM (Pattabiraman et al., 2015a). These stressors alter the biomechanical properties of TM tissue by increasing actin cytoskeletal tension, reorganization of cell adhesion complexes, and excessive rearrangement, accumulation, and decreased breakdown of extracellular matrix (ECM) components resulting in increased AH outflow resistance and elevated IOP (Vranka et al., 2015). Elevated IOP is a major risk factor for glaucoma, an irreversible blinding disease. Primary open-angle glaucoma (POAG), a form of glaucoma, is a highly prevalent type, and major public health concern in the United States as well as globally (Quigley & Broman, 2006).

Among the various stress response proteins, clusterin or Apolipoprotein J, is an ubiquitously expressed secretory chaperone protein (Trougakos, 2013). The clusterin (CLU) gene is located in region 8p21-p12 of the human chromosome 8, and it is widely expressed in various tissues (Aronow et al., 1993). Clusterin gene is made up of 9 exons, encoding for at least three different messenger RNA (mRNA) variants, namely clusterin variants −1, −2, and −3. The mRNAs contain a unique exon 1 but share exons 2–9 to make up the variants. The full-length clusterin mRNA encodes for the polypeptide of 449 amino acids. Clusterin has three isoforms with distinct subcellular locations—secretory form (sCLU), pre-secreted-glycosylated peptide (psCLU), and nuclear clusterin (nCLU) (Jeong et al., 2012). Mature clusterin is secreted as a heterodimeric protein (70–80 kDa) comprising of disulfide-linked α (34–36 kDa) and β (36–39 kDa) subunits and is one of only a few known extracellular chaperones acting outside the cell (Trougakos, 2013). Glycosylation of clusterin is an important regulator of its secretion and chaperone function (Dabbs & Wilson, 2014; Rohne et al., 2014). As a molecular

chaperone, clusterin counteracts proteotoxic stress by binding to intermediate folding states of the denaturing proteins, thereby preventing uncontrolled aggregation (Dabbs & Wilson, 2014; Trougakos, 2013; Wyatt et al., 2011). Furthermore, clusterin not only solubilizes misfolded proteins but also promotes their removal from extracellular space (Wyatt et al., 2011). Mechanical stress and TGFβ are known to regulate clusterin expression in various tissues (Michel et al., 1997; Urbich et al., 2000). Clusterin can bind to the membrane receptors, lipids, complement factors, and extracellular matrix (ECM) proteins but their function post-binding is not well characterized (Doudevski et al., 2014). Upregulation and down-regulation of clusterin can decrease and increase tissue fibrosis respectively (Peix et al., 2018). Studies have associated increased ECM deposition in TM with decreased AH outflow and IOP elevation (Kasetti et al., 2017; Keller et al., 2009; Pattabiraman & Toris, 2016). Clusterin is among the highly expressed genes in the TM (Liton et al., 2005). In a microarray study comparing glycogene expression profiles of whole TM tissues from normal and glaucomatous eyes obtained from human donors showed significant twofold reduction in clusterin mRNA in POAG (Diskin et al., 2006). Biochemical and interactome study on genes implicated in ocular hypertension has shown a putative linkage of the clusterin gene in the POAG pathogenesis (van Koolwijk et al., 2012). Yet there is no known cellular and molecular basis for the relationship between clusterin and its role in the regulation of IOP homeostasis. This study mechanistically explores the functional relevance of clusterin in the actin polymerization and ECM remodeling in the TM and on IOP regulation.

2 | MATERIALS AND METHODS

2.1 | Materials

Reagents and antibodies used in this study were procured from: R&D Systems—Human recombinant CTGF (#9190CC), anti-TSP-1 (#AF3074); Millipore Sigma—Human recombinant TGFβ2 (#GF440), Human recombinant endothelin1 (#E7764-50UG), and dexametha-sone (#265005-100MG), anti-Vinculin (#V9131), anti-β-actin (#A1798). AcroBiosystems recombinant human clusterin (rhCLU) (CLUH5227100UG); Proteintech Group Inc.—anti-elastin #15257-I-AP); Abcam—anti-collagen1α (#ab34710), anti-TGFβ2 (#ab36495); Santa Cruz Biotechnology—Tunicamycin (#sc3506A), anti-clusterin (#sc166907 and #sc6420), anti-PAI-1 (#sc5297), anti-MMP2 (#sc13595), anti-PRKD1 (#sc90039S), anti-LIMK1 (#sc515585), anti-PRK2 (#sc271971), anti-Plectin (#sc33649), anti-paxillin (#sc365379), anti-GAPDH (#sc-25778); NEB—PNGase F (#P0704S). Cell Signaling Technology—anti-phospho-Paxillin (#69363S), anti-Integrin αV (#4711P), anti-Integrin β3 (#4702P), anti-Integrin β5 (#4708P); Anti-fibronectin (gift from Dr. Harold Erickson, Duke University); and ThermoFisher Scientific—anti-Zo1 (#33-9100). Sec-ondary antibodies conjugated with horseradish peroxidase—Donkey-anti-goat IgG (705-035-003), anti-mouse IgG (#715-035-150), and

anti-rabbit IgG (#715-035-144)—were purchased from Jackson Immuno Research. Fluorescent dye conjugated secondary antibodies-Goat-anti-Mouse IgG Alexa Fluor Plus 488 (#A32723), anti-Mouse IgG Alexa Fluor Plus 594 (#A32742), anti-Rabbit IgG Alexa Fluor Plus 488 (#A32731), and anti-Rabbit IgG Alexa Fluor Plus 594 (#A32740)—were purchased from ThermoFisher. F-actin staining reagent Phalloidin (Alexa Fluor Plus 488 PHA, #A12379 and Alexa Fluor Plus 594 PHA, #A12381) was purchased from Invitrogen/ ThermoFisher.

2.2 | Human trabecular meshwork cell culture

Primary HTM cells were cultured from TM tissue isolated from the leftover donor corneal rings after they had been used for corneal transplantation at the Indiana University Clinical Service, Indianapolis, as described previously (Keller et al., 2018). HIPPA compliance guidelines were adhered for the use of human tissues. The usage of donor tissues was exempt from the DHHS regulation and the IRB protocol (1911117637), approved by the Indiana University School of Medicine IRB review board. The age, race, and sex of the donors were obtained from eye banks, which provided the corneas. TM tissue extracted from the corneal ring was chopped into fine pieces and placed in a 2% gelatin-coated six-well tissue culture plate sandwiched by a coverslip. The tissues were grown in OptiMEM (Gibco, #31985-070), containing 20% fetal bovine serum (FBS) and penicillin-streptomycin-glutamine solution (Gibco, #10378-016). The expanded population of HTM cells was sub-cultured after 1–2 weeks in Dulbecco's modified Eagle's medium, containing 10% FBS and characterized by detection of dexamethasone-induced myocilin. All experiments in this manuscript were performed using biological replicates. The normal TM (NTM5) cell line obtained from Dr. Weiming Mao, Indiana University School of Medicine, was cultured as mentioned above.

2.3 | Cell culture treatments

Overnight serum starvation was carried out on HTM cultures before treatments. Cells were subjected to TGFβ2 (5 ng/ml), endothelin1 (ENDO-1) (200 nM), CTGF (40 ng/ml), rhCLU (0.5 μg/ml), Dexamethasone (DEX) (100 nM), and Tunicamycin (TU) (1 μM) for 8–48 h. Post-treatment, cells were collected in TRIZOL for RNA isolation or in 1X radioimmunoprecipitation assay (RIPA) buffer for protein isolation along with the cell culture media and stored in −80°C until used.

2.4 | Deglycosylation

Deglycosylation of total protein was carried out using Peptide-N-Glycosidase F (PNGase F) following the manufacturer protocol. In brief, for each reaction, 20 μg of protein was initially denatured using glycoprotein buffer followed by heating at 100°C for 10 min. To this,

GlycoBuffer2 (10X), 10% NP-40, and PNGase F were added and incubated at 37°C for 1 h.

2.5 | Cyclic mechanical stretch

HTM cells were cultured in collagen-coated BioFlex plates (#BF-3001C) (Flexcell International, Burlington, NC); and after 90% confluency, the plates were fixed on a FlexCell (FX-6000 Tension System) (Flexcell International). The cells were stretched at 0.69 Hz frequency with 15% stretching for 8 h for gene expression analysis and 24 h for protein expression analysis based on previously published report (Luna et al., 2009). Cells and media were collected and processed further.

2.6 | Ex vivo elevated IOP model

Freshly enucleated porcine whole globes obtained were cleaned by trimming the extra-ocular muscle and immersing in povidone-iodine topical antiseptic solution (Betadine), followed by washes in 1x phosphate-buffered saline (PBS) solution. The globes were then cut below the limbus, and anterior segments with intact TM were prepared by removing the remnant of the vitreous humor, lens, ciliary body, and iris. The anterior segments were then mounted onto a custom-made perfusion chamber consisting of a foundational component and an O-ring. The foundational component consists of a convex mound with two cannulas that allow for an influx of fluid and its subsequent drainage to simulate the AH pathway. The column connected to the chamber was filled with 1X PBS containing 5.5 mM D-glucose, up to a height that corresponds to either 15 or 30 mmHg. A baseline pressure of 15 mmHg was first established for 30 min for all the eyes. One eye was subjected to 15 mmHg pressure, whereas the contralateral eye was subjected to a constant pressure of 30 mmHg for 5 h. Then TM was collected and processed for either RNA or protein as described below.

2.7 | Construction of replication-deficient recombinant adenovirus expressing clusterin

Generation of replication-defective recombinant adenovirus expressing secretory clusterin (AdCLU) was performed using ViraPower Adenoviral Expression System (#K4930-00; Invitrogen). Full-length clusterin (1344 bps) was amplified from high-fidelity PCR (Advantage-HF 2 PCR kit, #639123; Clontech) from human clusterin in pcDNA6 (a gift from Claudia Koch-Brandt, Johannes Gutenberg University of Mainz) (Rohne et al., 2014). The amplified product was gel extracted, purified, sequenced, and cloned into the pENTR/D-TOPO cloning vector (#K243520; Invitrogen). The pENTR construct generated was then recombined with the pAd/CMV/V5-DEST vector (#V493-20; Invitrogen), using Gateway technology and the LR Clonase II enzyme mix (#11791020; Invitrogen) to create the pAd-CMV-CLU. The

pAd-CMV-CLU was linearized by Pac 1 (#RO547S; New England Biolabs) digestion and transfected into 293A cells using Lipofectamine 3000 (Life Technologies) to produce recombinant adenoviruses expressing clusterin (AdCLU), which was subsequently amplified in 293A cells yielding crude lysates containing adenovirus particles and it was purified using Adeno-X™ Maxi Purification (#631533, Takara Bio). HTM cells were infected with 50 multiplicities of infection. A control empty virus (AdMT) a gift from Dr. Douglas Rhee, Case Western Reserve University; was also amplified and purified.

2.8 | Adenovirus-mediated gene transduction in HTM cells

Human TM cells were grown on gelatin-coated glass coverslips or in plastic petri dishes and were infected with either AdMT or AdCLU with 50 multiplicities of infection for 24 h followed by 48 h serum starvation. Cells were then washed with 1X PBS and were fixed for immunofluorescence analysis or collected using either TRIZOL for RNA extraction or 1X RIPA for protein extraction. Media was collected and concentrated using Nanosep® Centrifugal Devices with Omega™ Membrane 10 K (Pall, #OD010C34).

2.9 | Gene expression analysis

Total RNA was extracted from TM tissue and cells using the Trizol method following the manufacturer's protocol. The RNA amounts were quantified using NanoDrop 2000 UV-Vis Spectrophotometer (Thermo Scientific). Equal amounts of RNA were then reverse-transcribed to complementary DNA (cDNA) using the 5X All-In-One RT MasterMix (Applied Biological Materials Inc., #G492) with genomic DNA removal according to the manufacturer's instructions. The following reaction condition was maintained for cDNA conversion: incubation at 25°C for 10 min, followed by incubation at 42°C for 15 min, and enzyme inactivation at 85°C for 5 min. The cDNA was diluted as per requirement, and 10 µl was used for gene expression analysis using Quant Studio Flex 6/7 thermocycler (ThermoFisher Scientific). Bright Green 2X qPCR MasterMix-ROX (Applied Biological Materials Inc., #MasterMix-LR-XL) and gene-specific oligonucleotides (Integrated DNA Technologies) were used for the analysis. Sequence-specific forward and reverse oligonucleotide primers for the indicated genes are provided in Table 1.

Each sample for the PCR reaction was performed in triplicate using the following protocol: initial denaturation for 95°C for 2 min followed by 40 cycles of denaturation at 95°C for 15 s, annealing at 60°C for 15 s, and extension at 72°C for 1 min. An extended step was used to measure the melting curves obtained immediately after amplification by increasing the temperature in 0.4°C increments from 65°C for 85 cycles of 10 s each. The fold difference in expression of test genes between the control and treatment was calculated by the delta-delta Ct method. Normalization was performed using either hydroxymethylbilane synthase (HMBS) for PTM or glyceraldehyde-3-phosphate dehydrogenase (GAPDH) for HTM.

TABLE 1 Oligonucleotide primers used in the RT-PCR and qPCR amplification.

Total CLU	Forward	AAAATGCTGTCAACGGGGTG
	Reverse	TTCAGGCAGGGCTTACACTCT
CLU Transcript1	Forward	ACAGGGTGCCGCTGACC
	Reverse	CAGCAGAGTCTTCATCATGCC
GAPDH	Forward	TGCACCACCAACTGCTTAGC
	Reverse	GGCATGGACTGTGGTCATGAG
MMP2	Forward	ACTGTGACGCCACGTGAACCAA
	Reverse	CGTATACCGCATCAATCTTTCC
TIMP1	Forward	GCTTCACCAAGACCTACACTGTTG
	Reverse	CTGGTCCGTCCACAAGCAA
TIMP2	Forward	AAACGACATTTATGGCAACCCCTAT
	Reverse	GGGCCGTGTAGATAACTCTATATCC
Porcine HMBS	Forward	AGGATGGGCAACTCTACCTG
	Reverse	GATGGTGGCCTGCATAGTCT
Porcine CLU	Forward	GATGAAGGACCAGTGTGAGAAG
	Reverse	ATCTGAGAGGAATTGCTGGC

Abbreviation: qRT-PCR, quantitative reverse-transcription polymerase chain reaction.

2.10 | Protein analysis by immunoblotting

The cell lysates containing total protein were prepared using 1X RIPA buffer composed of 50 mM Tris-HCl (pH 7.2), 150 mM NaCl, 1% NP-40, 0.1% sodium dodecyl sulfate (SDS), 1 mM EDTA, and 1 mM PMSF with protease and phosphatase inhibitors (ThermoFisher Scientific, #A32961) and then sonicated. The protein concentration was determined using either the Bradford Assay Reagent/Bio-Rad Protein Assay Kit I (Bio-Rad, #5000001) or BCA protein assay (Thermo Fisher Scientific, #23338). A total of 20–40 µg of the protein sample was mixed with 4X Laemmli buffer and separated on 8%–15% SDS polyacrylamide gel. Following the gel run, the proteins were transferred to 0.45 µM pore size nitrocellulose membrane (GE Healthcare, #10600003). Ponceau S staining of the membrane was performed to document the protein loading after transfer. Membranes were blocked in 5% nonfat dry milk in Tris-buffered saline with 0.1% Tween for 2 h followed by respective primary antibodies overnight at 4°C (~16 h), and then by horseradish peroxidase-conjugated secondary antibodies (Jackson Immuno Research). The blots were washed with 1X Tris buffered saline with Tween-20, and the immunoreactivity was detected using Western Lightning Plus Enhanced Chemiluminescence (ECL) Substrate (Perkin Elmer) and imaged using ChemiDoc MP imaging system (Bio-Rad). Blots were stripped using mild stripping buffer if required to reprobe for the loading control and multiple proteins within the same molecular weight range. The data were normalized to GAPDH or β-actin. Semi-quantitative analyses and fold changes were calculated from the band intensities measured using Image J software.

2.11 | Immunofluorescence staining

Tissue sections from formalin-fixed, paraffin-embedded human donor whole globe eyes were prepared at Case Western Reserve University. Paraffin-embedded porcine TM tissue slides were prepared at the Histology Core, Indiana University, and immunolabeling was performed. Briefly, five-micron thick tissue sections were deparaffinized in xylene for 15 min and incubated with xylene for a second 15 min period. The sections were subsequently hydrated with ethanol dilutions (100%, 95%, and 70%). To unmask the antigen epitopes, heat-induced antigen retrieval was performed using 0.1 M citrate buffer pH 6.0 (Vector Laboratories) for 20 min at 100°C. The slides were then blocked for nonspecific interactions with Sniper Background Reducer (#BS966H) (Biocare Medicals). For immunohistochemical staining, hematoxylin and eosin staining were performed using Hematoxylin and Eosin Stain kits (Vector Laboratories, Inc.). For immunofluorescence staining, the primary antibody was used at 1:100 dilution overnight at 4°C. The slides were subsequently washed with 1×PBST, and secondary antibodies were applied at 1:200 for 1 h in room temperature. After two additional washes, the coverslips were mounted with Fluoroshield mounting medium with 4′,6-diamidino-2-phenylindole (DAPI) (Abcam, #ab104139). For staining, a minimum of two slides per ocular tissue sample were utilized, with each slide containing three consecutive sections from the same eye. This was repeated across the biological replicates tested.

HTM cells were grown on 2% gelatin-coated glass coverslips until they attained 90% confluency. After appropriate treatment, cells were washed with 1X PBS twice, fixed in 4% paraformaldehyde for 20 min, permeabilized with 0.2% triton-x-100 in PBS buffer for 10 min, and blocking with 5% bovine serum albumin in 1X PBS for 1 h. Cells were then incubated with the respective primary antibody overnight at 4°C. After washing three times with 1X PBS, they were incubated in Alexa fluor-conjugated secondary antibodies for 1 h at room temperature. Finally, the coverslips were washed and mounted onto glass slides with Fluoroshield Mounting Medium (Abcam, #ab104139). The slides were imaged under a Leica DMI 6000 B inverted microscope and a Retiga EXi Aqua Blue camera (Q-imaging) or Zeiss LSM 700 confocal microscope, z-stack images were obtained, and processed using Zeiss ZEN image analysis software.

2.12 | Live cell imaging to determine the regulation of clusterin by TGFβ2

Clusterin-red fluorescent protein (RFP)—green fluorescent protein (GFP) (CLU-RG) or signal peptide-RFP-GFP (SP-RG) plasmid (generous gift from Dr. Eisuke Itakura, Chiba University, Japan) (Itakura et al., 2020) was transfected in NTM5 cells using Lipofectamine 3000 (Invitrogen, #L3000-015) as per manufacturer protocol. Post 48 h, live-cell time-lapse imaging before and after TGFβ2 (5 ng/ml) addition was performed using a Zeiss LSM 700 confocal microscope attached to a Tokai Hit Stage Top Incubator. RFP and GFP fluorescence signals were recorded.

2.13 | Assessment of MMP activity using zymography

After treating HTM cells with AdCLU, the conditioned media was collected and concentrated. Equal volume of media was mixed with 2X non-reduced Laemmli sample buffer and separated by SDS-polyacrylamide gel electrophoresis containing 0.2% gelatin. The gel was renatured using 2.5% triton-x100. Gels were incubated overnight (16–18 h) at 37°C in 50 mM Tris-HCl [pH 7.5], 200 mM NaCl, 5 mM $CaCl_2$, 0.05% NaN_3. The gel staining was carried out using 0.1% (w/v) Coomassie blue in staining/destaining buffer (Water: acetic acid: methanol-4.5:1:4.5) for 1.5 h. Destaining was performed using staining/de-staining solution for approximately 2 h or until white bands are observed in clear background, which was imaged using ChemiDoc MP imaging system (Bio-Rad).

2.14 | Clusterin knockout mice

All experiments were performed in compliance with the Association for Research in Vision and Ophthalmology (ARVO) Statement for the Use of Animals in Ophthalmic and Vision Research. Mice with heterozygous deletion of clusterin (C57BL/6J background) were obtained from Dr. John Fryer (Mayo Clinic, Florida) and housed under a standard 12 h light and dark cycle with food and water provided ad libitum. All animal procedures were approved by the Institutional Animal Care and Use Committee at the Case Western Reserve University and Indiana University School of Medicine and conducted in accordance with the Declaration of Helsinki. Heterozygous mice were utilized for breeding. The wild type and knockout littermates were used for the experiments. A total of 12 animals were used in this study for IOP measurement with six wild-type and six knockout mice.

2.15 | Measurement of IOP

The mice were anesthetized by intraperitoneal (IP) injection of a ketamine/xylazine mixture (100 and 9 mg/kg body weight respectively). A previously validated commercial rebound tonometer (TonoLab; Colonial Medical Supply) was used to take three sets of six measurements of IOP in each eye. The IOP measurements were carried out in a blinded manner by the experimenter to minimize outcome bias. Right and left eye measurement sets were alternated with the initial eye selected randomly. All measurements were taken between 4 and 7 min after IP injection based on prior studies. As indicated by the manufacturer, the tonometer was fixed horizontally for all measurements, and the tip of the probe was 2–3 mm from the eye. To reduce variability in measurements, the tonometer with a modified pedal that activates the probe without the need for handling the device was utilized. The probe contacted the eye perpendicularly over the central cornea. The average of a set of measurements was accepted only if the device indicated that there was "no significant

variability" (as per the protocol manual; Colonial Medical Supply). Daytime measurements were taken between 11:00 and 15:00 h. IOP was measured in the littermates at 50 days and 90 days postbirth.

2.16 | Statistical analysis

For in vitro experiments, all data presented was based on four to six independent observations. The graphs represent the mean ± standard error. All statistical analyses were performed using Prism 8.1.1 (GraphPad). The difference between two groups was assessed using paired and unpaired Student's t tests when parametric statistical testing was applicable. When multiple groups were compared, one-way analysis of variance followed by Tukey post hoc test was applied. The p value ≤ 0.05 was considered a statistically significant difference between test and control samples.

3 | RESULTS

3.1 | Clusterin is expressed in the human TM outflow pathway and secreted into aqueous humor

Clusterin isoforms present in TM were profiled using reverse-transcription polymerase chain reaction (RT-PCR) with total RNA extracted from two different biologically independent primary HTM cell cultures. The analysis demonstrated the expression of the transcript 1 (NM_001831.4) (Figure 1a), which gives rise to the secretory clusterin (Prochnow et al., 2013). The other isoforms including the cytoplasmic or the nuclear forms were not found in HTM cells under the basal conditions tested. The clusterin protein expression in HTM cells and secretion into cell culture media as well as AH was tested on the protein extracted from primary HTM whole cell lysate (WCL), in conditioned media (CM), and in AH using immunoblotting, on a reducing gel. We observed a band at ~70 kDa in the WCL (Figure 1b). In the CM, we found one prominent band at ~70 kDa and a fainter band slightly higher (Figure 1b). In the AH, we found two slightly higher bands close to ~80 kDa potentially indicating differentially glycosylated forms secreted into AH from various tissues in the anterior segments (Figure 1b). These were all confirmed to be differentially glycosylated forms of clusterin (Figure S1) (denoted by asterisk in the decreased exposure blot) because upon PNGase F treatment to deglycosylate the N-glycosylation, we found a single band at ~52 kDa indicating the nascent clusterin. Followed by the verification of clusterin expression and secretion, we performed immunofluorescence analysis and confocal imaging on HTM cells and human TM AH outflow pathway to identify clusterin distribution. The clusterin distribution in the HTM cells showed vesicular and speckled distribution in the cytosol (Figure 1c) and was found distributed in the anterior chamber angle of a normal human eye with immune-positive cells for clusterin in the TM-JCT region and in the endothelial cells lining the SC, and DAPI (blue) staining the nucleus (Figure 1d left panel). Negative control in the presence of secondary antibody alone did not show any staining (Figure 1d right panel).

3.2 | Clusterin expression and secretion are negatively regulated by stressors in TM known to elevate IOP

Among the various functions of clusterin, the role of a stress response chaperone protein is of prime importance (Poon et al., 2000). To explore the influence of stress on clusterin expression and its secretion in TM, we subjected HTM cells to various stressors documented to elevate IOP and result in POAG. The TM tissue is constantly subjected to mechanical stress due to cyclic changes in the IOP that is induced by the cardiac pulse (Li et al., 2013). Therefore, we investigated the effects of mechanical stress such as cyclic mechanical stretch (CMS) (Luna et al., 2009) and acute pressure elevation stress on clusterin expression levels. The HTM cells were subjected to CMS and both gene and protein expression for clusterin were analyzed. No significant changes were observed in clusterin mRNA expression levels (Figure 1e). However, clusterin protein expression significantly decreased ($n = 4$, $p = 0.02$) in both whole cell lysate (WCL) (Figure 1f) and conditioned media (CM) (Figure 1g) in response to CMS. To achieve pressure stress—porcine anterior segments were subjected to two times elevated pressure. Under elevated pressure stress (30 mmHg), we found a significant down-regulation of clusterin mRNA ($n = 7$, $p = 0.01$) (Figure 1h) and protein expression ($n = 4$, $p = 0.02$) (Figure 1i). Additionally, we explored the effects on clusterin expression and secretion by stressors including—CTGF, ENDO-1, DEX, and TGFβ2—in HTM cells in vitro. Figure 2a,b represents the time-dependent study with a constant dose treatment of stressors. (a) ENDO-1 resulted in significant decrease ($p = 0.01$) in clusterin expression at 24 h in the WCL and at 24 h ($p = 0.05$) and 48 h ($p = 0.01$) in the CM, (b) CTGF resulted in a significant reduction ($p = 0.04$) in the WCL at 24 h, and (c) DEX significantly decreased ($p = 0.02$) the secretory clusterin levels in CM at 24 h. Though TGFβ2 did not show a significant change in clusterin levels at 24 h or 48 h, however, there was a downward trend in the clusterin levels at 24 h both in WCL and CM. Thus, suggesting downregulation of clusterin under the influence of TGFβ2.

Endoplasmic reticulum (ER) stress is a pathological mechanism resulting in elevated IOP and reversal of ER stress can lower ocular hypertension (Kasetti et al., 2017). Clusterin is a glycosylated stress response chaperone protein. We found that ER stress induced by tunicamycin decreased the levels of clusterin protein (Figure 2c) and induced significant deglycosylation of clusterin in a time and dose-dependent manner as identified by the deglycosylated bands at ~50 kDa. The confirmation of deglycosylation was achieved using PNGase F treatment of the same samples resulting in clusterin bands at the ~50 kDa. The secretion of the mature and the heterodimeric clusterin was significantly decreased ($p < 0.01$ and $p < 0.001$) due to ER stress induced by tunicamycin (Figure 2d). Therefore, indicating that clusterin production, secretion, and degradation are altered
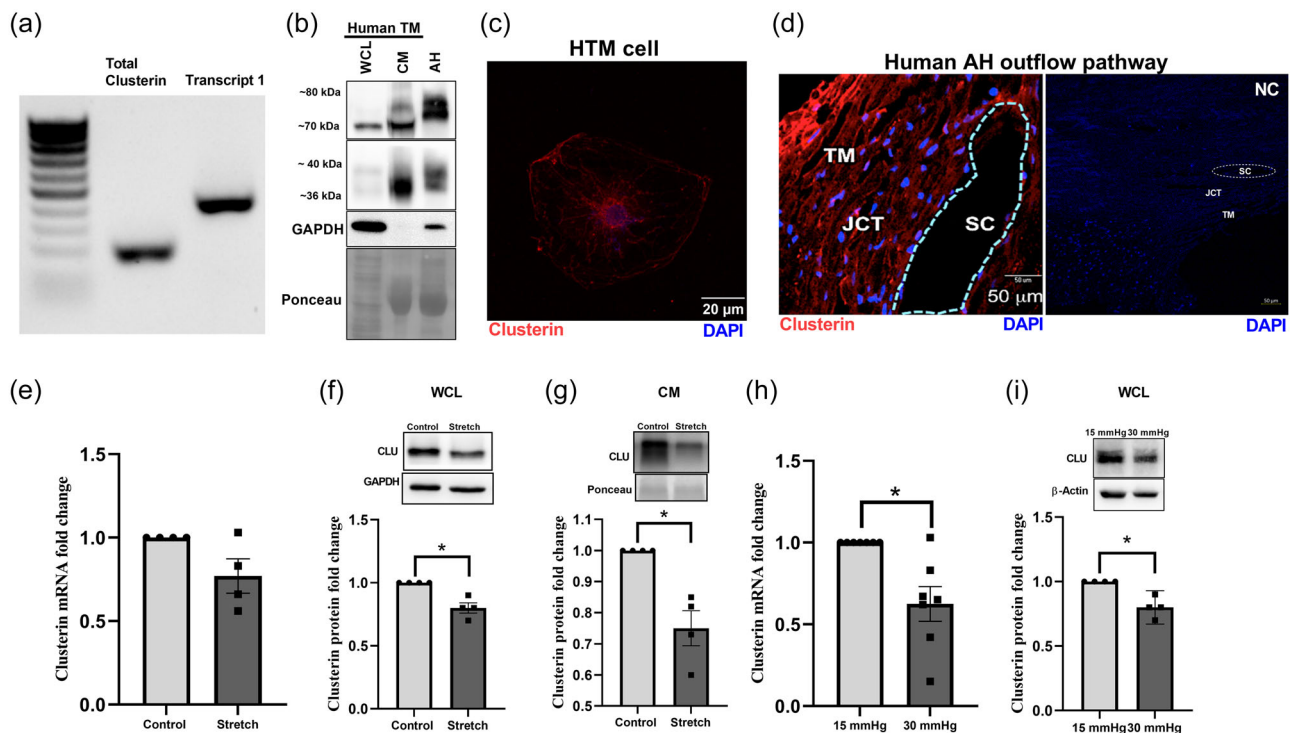
FIGURE 1 Expression, distribution, and regulation of clusterin in human AH outflow pathway.
(a) Expression profile of clusterin isoforms in TM cells by reverse-transcription polymerase chain reaction (RT-PCR) showing transcript 1 that gives rise to secretory clusterin in HTM. (b) Protein expression of clusterin in primary HTM cells (donor aged 69 y, male, Caucasian)-whole cell lysate (WCL) and conditioned media (CM), and in AH from a human donor eye (donor aged 60 y, male, Caucasian). Clusterin is seen at ~70 kDa along with its heterodimers seen at 36–40 kDa in WCL. Mature secretory clusterin was seen at ~70–80 kDa in both CM and AH along with 36–40 kDa heterodimers. GAPDH was used as the loading control for cell lysate, and Ponceau S band was used for CM and AH.
(c) Immunofluorescence (IF) showing the cytosolic distribution of clusterin (red puncta) in primary HTM cell. The nucleus was stained with DAPI in blue. Images were captured in z-stack in a confocal microscope, and stacks were orthogonally projected. Scale bar 20 microns. (d) Tissue distribution of clusterin in the AH outflow pathway of a normal human eye specimen by IF. The representative image shows the clusterin distribution (red) in the TM-JCT region and in the inner wall of SC. DAPI was stained in blue. The negative control (in the presence of secondary antibody alone did not show any significant staining (right panel). Images were captured in z-stack in a confocal microscope, and stacks were orthogonally projected. Scale bar 50 microns. (e–i) Regulation of clusterin mRNA and protein expression by mechanical stress. (e) mRNA expression showed no significant change. (f and g) Protein levels in WCL and CM was significantly reduced in HTM cells subjected to cyclic mechanical stretch compared to nonstretched control. (h) mRNA and (i) protein expression in WCL significantly reduced in TM derived from enucleated porcine anterior segments perfused under the elevated pressure of 30 mmHg for 5 h compared with 15 mmHg. The results were based on semi-quantitative immunoblotting with subsequent densitometric analysis. GAPDH and HMBS for HTM and PTM, respectively, were used as internal controls for qPCR analysis. GAPDH, β-actin, or ponceau was used as a loading control for immunoblotting analysis. Values represent the mean ± SEM, where $n = 4$–7 (biological replicates). *$p \leq 0.05$ was considered significant. AH, aqueous humor; DAPI, 4′,6-diamidino-2-phenylindole; mRNA, messenger RNA; SEM, standard error of mean; TM, trabecular meshwork

under ER stress. Interestingly, the role of TGFβ2 on inducing unfolded protein response (UPR) due to endoplasmic reticulum (ER) stress in TM has been established (Kasetti et al., 2018). Under stress, the ER, which is the hub of protein biogenesis in the secretory pathway, can triage the misfolded proteins to the lysosome/vacuole through ER-associated degradation (ERAD) or ER-phagy. Therefore, to understand the regulation of the life of clusterin by TGFβ2, we performed live-cell imaging of CLU-RG or the control SP-RG before and after TGFβ2 treatment in NTM cells using confocal microscope. Images were taken before (baseline) and after TGFβ2 treatment at three different time intervals (2.5, 5, and 8 h). The CLU-RG and SP-RG produce both green and red fluorescence which tend to colocalize under normal circumstances. However, under acidic environments

such as in the lysosomal vesicles, the target protein and GFP gets degraded via the lysosomal enzymatic degradation sparing RFP, which is highly resistant to the acidic environment (Itakura et al., 2020). Therefore, increased RFP puncta visualization implies a degradation of the protein in question. Figure 2e shows image of a single cell per treatment condition. Each condition is presented with GFP panel (left), RFP (middle), and merge (right). The top two panels comprise of cell transfected with SP-RG before (first row panels) and after TGFβ2 treatment (second-row panels). Third and fourth panels comprise cell transfected with CLU-RG before (third-row panels) and after TGFβ2 treatment (panel in fourth row) (Figure 2e). A quantitative assessment of the number of red and green puncta was carried out in 11 cells for SP-RG and 14 cells for CLU-RG across
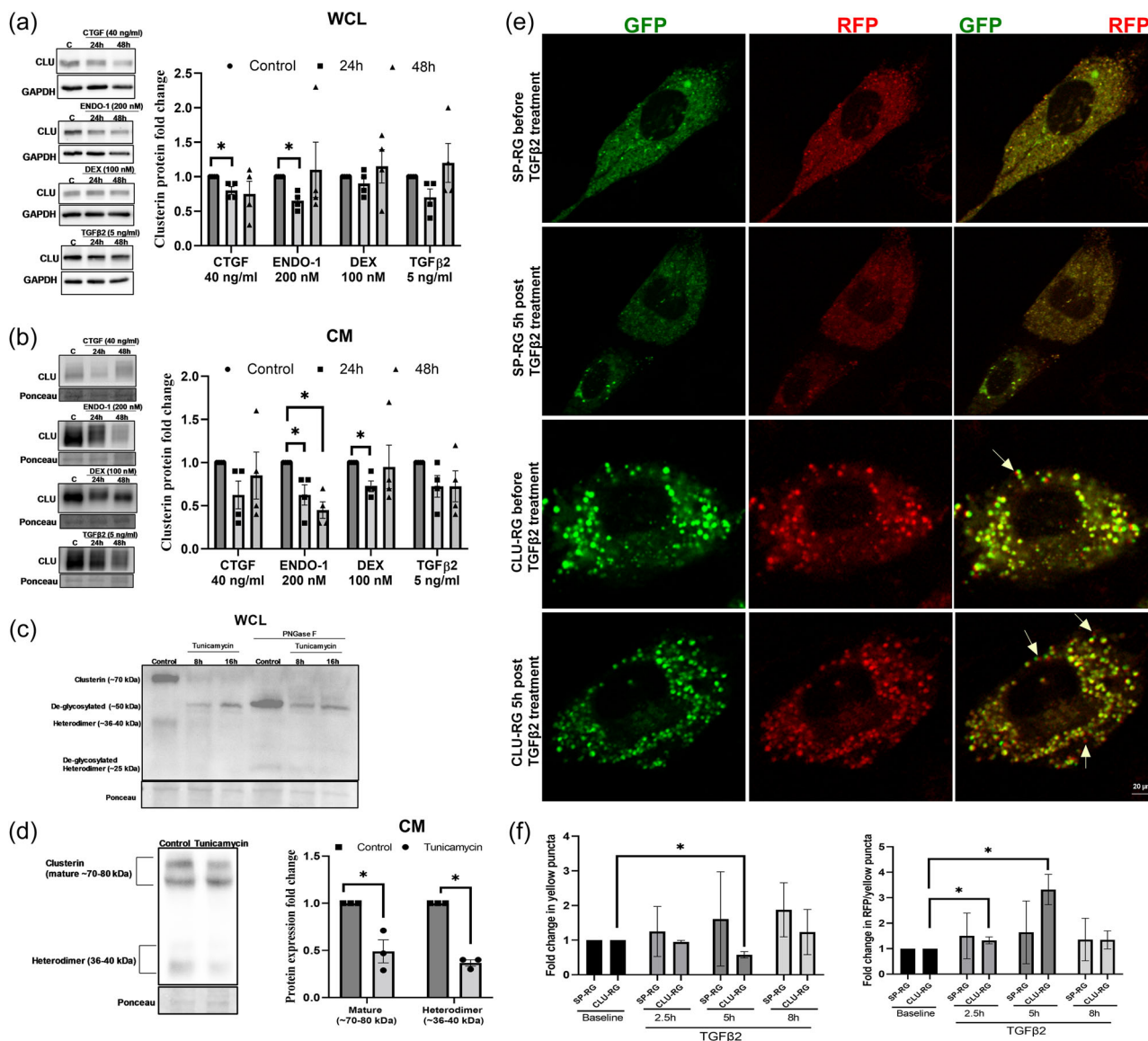
FIGURE 2 Regulation of clusterin expression levels by stressors involved in modulating IOP. (a and b) Clusterin protein levels in response to 24 and 48 h treatment of connective tissue growth factor (CTGF)-40 ng/ml, endothelin-1 (ENDO-1)-200 nM, steroid dexamethasone (DEX)-100 nM, transforming growth factor β2 (TGFβ2)-5 ng/ml in WCL and CM. Clusterin expression was significantly reduced in WCL of HTM cells treated with CTGF and ENDO-1 for 24 h. In CM, both 24 h and 48 h treatment of ENDO-1 and 24 h treatment of DEX significantly reduced clusterin levels. (c) Effect of ER stress on clusterin expression. 1 μm tunicamycin treatment for 8 h and 16 h deglycosylated clusterin (~50 kDa). Peptide-N-glycosidase F (PNGase F) treatment on control and tunicamycin treated protein samples were used as positive controls for deglycosylation. PNGase F treated protein samples showed deglycosylated clusterin band at ~50 kDa and deglycosylated heterodimer band at ~25 kDa. (d) Tunicamycin treatment resulted in significant reduction in both mature secretory clusterin (~70–80 kDa) and heterodimer (~36–40 kDa). (e) Effect of TGFβ2 on bioavailability of clusterin. NTM cell lines were transfected with plasmid expressing either Clusterin-RFP-GFP (CLU-RG) plasmids or control Signal Peptide-RFP-GFP (SP-RG), followed by TGFβ2 treatment (5 ng/ml) after 48 h. Live-cell imaging under confocal microscope was performed. Images were recorded before (baseline) and after TGFβ2 treatment (2.5, 5, and 8 h). Representative image of NTM cell for each condition is shown with GFP panel (left), RFP (middle), merge (right). Top two panels show cell transfected with SP-RG before (panel in first row) and after TGFβ2 treatment (panel in second row). Third and fourth panel show cell transfected with CLU-RG before (panel in third row) and after TGFβ2 treatment (panel in fourth row). Yellow arrows point towards red fluorescence puncta. Scale bar 20 microns. (f) Graphical representation of fold changes in fluorescence puncta. Fold changes in the ratio of colocalization (yellow puncta) (left panel) shows a significant decrease in yellow puncta fold change in CLU-RG transfected cells at the 5 h post-TGFβ2 treatment compared to the CLU-RG baseline with no changes in fold change in the SP-RG and RFP over colocalization (right panel) showed significant increase at 2.5 h and 5 h post-TGFβ2 treatment. GAPDH or ponceau was used as a loading control for immunoblotting analysis. Values represent the mean ± SEM, where n = 3–4 (biological replicates). * p ≤ 0.05 was considered significant. CM, conditioned media; GFP, green fluorescent protein; IOP, intraocular pressure; RFP, red fluorescent protein; SEM, standard error of mean; WCL, whole-cell lysate

the experimental conditions tested. Since the fold changes in the ratio of colocalization (Figure 2F, left panel) and RFP over colocalization (Figure 2f, right panel) are calculated before and after TGFβ2 treatment, the small difference in the cell count between SP-RG and CLU-RG will have minimal effect. We found a significant decrease ($n = 14$, $p = 0.001$) in fold change in yellow puncta in CLU-RG transfected cells only at the 5 h post-TGFβ2 treatment compared to the CLU-RG baseline with no changes in fold change in the SP-RG control before and after TGFβ2 treatment (Figure 2f, left panel). This decrease in colocalization indicated that there is loss of clusterin via degradation in the lysosomes induced by TGFβ2 treatment in a time-dependent manner. This was further confirmed by the significant increase in the ratio of RFP over colocalization in CLU-RG transfected cells both 2.5 and 5 h post-TGFβ2 treatment (Figure 2f, right panel). The ratio of RFP/colocalization in cells transfected with CLU-RG significantly increased after TGFβ2 treatment at 2.5 h ($n = 14$, $p = 0.01$) and 5 h ($n = 14$, $p = 0.002$) compared to CLU-RG transfected baseline (Figure 2f, right panel). These results suggest that TGFβ2-mediated stress on ER and protein synthesis machinery can shuttle clusterin for lysosomal degradation.

All the HTM cell strains used in this study collectively responded to the stressors by downregulating clusterin potentially resulting in loss of clusterin function.

3.3 | Functional loss of clusterin in TM resulted in increased expression as well as recruitment of actin cytoskeletal contractile machinery and its associated proteins

To study the loss of clusterin function in TM in vitro, we utilized siRNA-mediated knockdown of clusterin. HTM cells were either transfected with siRNA for scramble control (siScr) or siRNA for clusterin (siCLU). Firstly, we established that siCLU significantly decreased clusterin mRNA expression ($n = 4$, $p = 0.0001$) (Figure 3a). siCLU significantly decreased clusterin levels in WCL ($n = 4$, $p = 0.005$) (Figure 3b) and CM ($n = 4$, $p = 0.0001$) (Figure 3c). Upon examining the HTM cells posttransfection with siCLU, we found that siCLU induced cell shape changes (Figure 3d). A careful qualitative examination of the HTM cells under the phase-contrast microscope revealed that the siCLU transfected HTM cells were smaller and showed increased large cellular protrusions (Figure 3d, inset). To quantify these changes, we counted a total of 100 cells in siScr and 137 cells in siCLU from three different fields in three different coverslips. We found that 73/137 cells in siCLU condition showed protrusions compared with 5/100 cells in siScr (Figure 3d) and this was statistically significant ($p = 0.0006$). Furthermore, immuno-fluorescence analysis (Figure 3e) showed reduction in clusterin distribution (in red) due to siCLU compared with siScr. Thus, establishing that siCLU significantly decreased clusterin expression, distribution, and secretion. To confirm if the cell shape changes were because of actin cytoskeletal changes due to loss of clusterin and not an artifact introduced by lipofectamine reagent used in transfection,

we studied the changes in actin fiber organization and focal adhesion localization. Concomitantly, we found that in siCLU transfected HTM cells (Figure 3f,g bottom panels), there was an increase in actin fibers as well as cortical actin (red staining) (Figure 3f,g) and notable redistribution of focal adhesion proteins (green staining) including paxillin (Figure 3f) and vinculin (Figure 3g) to the focal contacts/edges of actin fibers as well as to the cellular protrusions compared with siScr (Figure 3f,g top panels). The nucleus was stained with DAPI (blue).

Further to decipher the mechanistic role of clusterin in modulating the actin cytoskeletal dynamics, we studied the influence of siCLU on the changes in protein expression involved in the regulation of actin contractile machinery in HTM cells in vitro. Since we found increased actin fibers, first we analyzed proteins involved in F-actin polymerization and stabilization. Protein kinase D1 (PRKD1), Protein kinase C- related protein kinase 2 (PRK2), and LIM domain kinase 1 (LIMK1) are targets of small GTP binding protein Rho and are involved in polymerization and stabilization of the actin fibers (Bernard, 2007; Eiseler et al., 2010; Vincent & Settleman, 1997). Western blot analysis showed a significant increase in PRKD1 ($n = 4$, $p = 0.007$), PRK2 ($n = 4$, $p = 0.02$), and LIMK1 ($n = 4$, $p = 0.03$) in siCLU compared with siScr (Figure 3h). Additionally, the clusterin loss significantly increased the levels of plectin, an actin linker-protein ($n = 4$, $p = 0.05$). Moreover, we found that siCLU induced an increase in paxillin levels ($n = 4$, $p = 0.001$) and its tyrosine 118 phosphorylated form (p-paxillin) ($n = 4$, $p = 0.0003$) (Figure 3h) indicating the increased cell adhesiveness and induction of cellular contractility. Since we found the paxillin and phospho paxillin to increase significantly, we calculated their pairwise ratio and found that the mean ratio was greater than 1 (1.26) but did not achieve significance (Figure 3h).

Finally, to define if such induction in actin-cell adhesive interactions resulted in changes in integrin levels augmenting cell-ECM interactions, we assayed for integrin (INT)-αV, -β3, and -β5. Our study found a significant increase in INTαV ($n = 4$, $p = 0.05$) and INTβ5 ($n = 4$, $p = 0.05$) in siCLU compared with siScr (Figure 3i).

3.4 | Total loss of clusterin resulted in elevated IOP

Increased actin cytoskeleton-mediated TM contraction results in decreased AH drainage and elevated IOP (Pattabiraman et al., 2015b). To test the functional role of the clusterin on IOP regulation, we measured the IOP in $Clu^{-/-}$ mice. The IOP was measured in anesthetized $Clu^{-/-}$ mice after 50-, 70-, 90-, and 105-days post-birth. Though there was no significant difference in IOP by 50 days but the $Clu^{-/-}$ mice displayed a mean higher IOP (16.08 ± 0.21 mmHg [mean ± SEM; $n = 6$]) compared with wild type (14.85 ± 0.19 mmHg [mean ± SEM; $n = 6$]) (Table 2). Further the IOP measurements at 70-, 90-, and 105- days demonstrated a significant IOP elevation in $Clu^{-/-}$ compared with WT by 70- ($n = 6$; $p = 0.004$), 90- ($n = 6$; $p = 0.0001$), and 105-days ($n = 6$; $p = 0.0001$) post-birth (Figure 3j). Interestingly, the percentage change in the difference in IOP (ΔIOP %) (Table 2) was up by 26% at 105 days
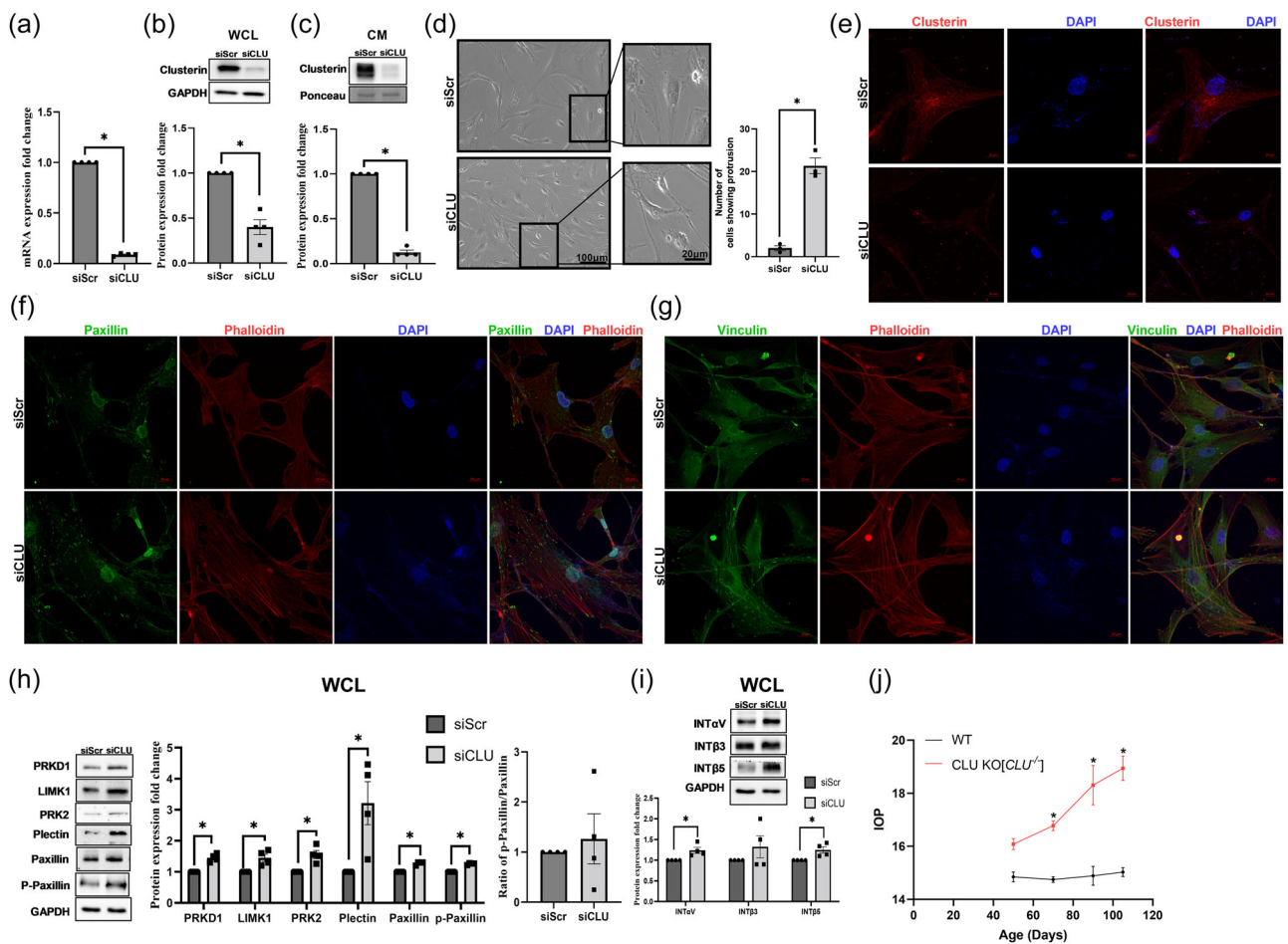
FIGURE 3 Effect of functional loss of clusterin on actin cytoskeleton and IOP. siRNA-mediated knockdown of clusterin (siCLU) in serum-starved HTM cells compared to control scramble (siScr) shows significant decrease in (a). clusterin mRNA, (b) clusterin protein levels in WCL, and (c) in CM GAPDH was used as a loading control for WCL, and Ponceau S-band at 55 kDa was used for the CM. (d) Changes in cell shape due to siCLU (bottom panel) were compared to siScr (top panel) observed using light microscopy. Scale bar 100 microns. The inset panels represent the zoomed in image. Scale bar 20 microns. Histogram on the right represents the quantitative assessment of cell shape change based on the number of protrusions. (e) Reduced clusterin distribution (Alexa Flour 568/red) (bottom panel) due to siCLU compared with siScr (top panel). The nucleus was stained with DAPI in blue. Images were captured in z-stack in a confocal microscope, and stacks were orthogonally projected. Scale bar 20 microns. (f and g) Increased distribution of actin stress fibers stained by phalloidin (red) with (f). paxillin, and (g) vinculin (Alexa Flour 488/green) seen in siCLU compared with siScr. The nucleus was stained with DAPI in blue. Images were captured in z-stack in a confocal microscope, and stacks were orthogonally projected. Scale bar 100 microns. (h) and (i) Changes in the levels of actin cytoskeleton-associated proteins due to loss of clusterin expression. Western blot analysis showed significant increase in the PRKD1, LIMK1, PRK2, plectin, paxillin, and phosphorylated paxillin. Ratio of phosphorylated paxillin to total paxillin demonstrated an increasing trend with no significance. Integrin- INTαV, INTβ5 showed significant increase in siCLU compared with siScr with no changes in INTβ3. GAPDH was used as a loading control for immunoblotting analysis. Values represent the mean ± SEM, where $n = 4$ (biological replicates). $*p ≤ 0.05$ was considered significant. (j) IOP values of wildtype (WT) and clusterin knockout ($Clu^{-/-}$) mice. Significant IOP elevation is observed in $Clu^{-/-}$ compared with WT by 70 days and continued over 90 and 105 days postnatal with no changes by 50 days. Data represented as mean ± SEM from 6 pairs of eyes ($n = 6$). $*p ≤ 0.05$ indicates statistical significance. IOP, intraocular pressure; mRNA, messenger RNA; SEM, standard error of mean

post-birth with a difference in IOP (ΔIOP) of 3.91 mmHg in $Clu^{-/-}$ mice compared with the wild type. Thus, indicating an effect of loss of clusterin function on IOP.

These results demonstrate that the loss of clusterin can potentially induce the actin cytoskeleton-based force-generation system in the TM in conjunction with increased integrin levels and possible recruitment to enhance ECM binding and reorganization leading to elevated IOP.

3.5 | Gain of function of clusterin results in loss of the contractile machinery and loss of cell-ECM interactions by negatively regulating the pro-fibrotic response

We investigated the effects of secretory clusterin on the contractile properties of the TM by utilizing AdCLU in primary HTM cells in vitro. Serum starved HTM cells were either treated with AdCLU or AdMT

	Age (days)			
_n_ = 6 (12 eyes in each)	50	70	90	105
WT IOP (mmHg) (mean ± SEM)	14.85 ± 0.19	14.75 ± 0.11	14.89 ± 0.36	15.03 ± 0.17
Clu$^{-/-}$ IOP (mmHg) (mean ± SEM)	16.08 ± 0.21	16.78 ± 0.18	18.31 ± 0.74	18.94 ± 0.46
Significance (_p_-value)	0.39	0.004	0.0001	0.0001
ΔIOP [Clu$^{-/-}$ - WT] (mmHg)	1.24	2.03	3.41	3.91
ΔIOP % [100 × (Clu$^{-/-}$ IOP – WT IOP)/WT IOP]	8.35	13.76	22.9	26.01

Abbreviations: IOP, intraocular pressure; WT, wild-type.

control. First, we established that AdCLU increased clusterin mRNA expression significantly ($n = 4$, $p = 0.05$) (Figure 4a), the clusterin protein expression in the WCL ($n = 4$, $p = 0.04$) (Figure 4b), and the secretion of clusterin in the CM ($n = 4$, $p = 0.009$) (Figure 4c) compared to AdMT. Further, immunofluorescence imaging for clusterin (Figure 4d) (in red) showed an increased clusterin distribution in vesicular structures due to AdCLU (bottom panel) compared with AdMT (top panel).

To determine if overexpression of clusterin alters actin cytoskeleton contractile machinery, we analyzed the changes in the protein expression levels of molecular machinery involved in actin polymerization and stabilization under the influence of AdCLU in serum starved HTM cells. We found that AdCLU significantly downregulated (Figure 4e) the actin regulatory and binding proteins including PRK2 ($n = 4$, $p = 0.0006$), and LIMK1 ($n = 4$, $p = 0.04$) compared with AdMT. Concomitantly, we found that the tight junction protein zonula occludens-1 (ZO-1) was significantly reduced ($n = 4$, $p = 0.007$) in AdCLU along with the integrins-INTαV ($n = 4$, $p = 0.04$) and INTβ5 ($n = 4$, $p = 0.01$) showing significant reduction compared to AdMT (Figure 4e). Thus, providing evidence for increased secretory clusterin inducing TM relaxation by lowering actin-based tension.

The loss of contractile forces due to a deficient actin-adhesome assembly can negatively regulate the ECM organization (Pattabiraman et al., 2014). To evaluate the effects of increased clusterin expression on ECM remodeling, we determined the effects of AdCLU on the changes in the levels and distribution of ECM and pro-fibrotic proteins. Under the influence of AdCLU on serum starved HTM cells and examining the levels of intracellular and secretory ECM and profibrotic protein expression, in the WCL there was a significant reduction in COL1A ($n = 4$, $p = 0.04$), FN ($n = 4$, $p = 0.03$), ELN ($n = 4$, $p = 0.005$), TGFβ2 ($n = 4$, $p = 0.03$), and TSP-1 ($n = 4$, $p = 0.005$) (Figure 5a). In the CM, the secretory FN ($n = 4$, $p = 0.002$), PAI-1 ($n = 4$, $p = 0.007$) and TSP-1 ($n = 4$, $p = 0.05$) showed significant reduction in AdCLU compared to AdMT (Figure 5b).

Since we found that the expression of proteins involved in actin polymerization/stabilization (Figure 4e) and the ECM protein levels were decreased with AdCLU, we assessed the changes in the F-actin fibers and ECM distribution in HTM cells under the influence of AdCLU. Immunofluorescence labeling for clusterin 72 h after AdCLU

transduction in HTM cells (Figure 5c) demonstrated an increase in clusterin distribution (in red) (left bottom panel) compared to AdMT (left top panel). In the AdCLU expressing HTM cells, there was marked decrease in F-actin fibers (in green) (bottom middle panel) as visualized by phalloidin labeling and comprehensive decrease in the immunolocalization and distribution of COL1A (in red) (bottom middle panel) and FN (in green) (bottom right panel) compared to AdMT (Figure 5c). These results demonstrate a significant decrease in the quantitative and qualitative changes of cytoskeleton-ECM interaction in TM due to an increase in secretory clusterin.

3.6 | Clusterin aids in the activation of MMP-2 to bring about the ECM lowering effects

Matrix metalloproteinase (MMPs) plays an important role in ECM remodeling and is suggested as a therapeutic approach to lower IOP (Weinreb et al., 2020). Since we found that clusterin negatively regulates ECM and clusterin is known to alter MMP activity in other tissues (Jeong et al., 2012), we wanted to provide the mechanistic evidence for ECM remodeling by clusterin in HTM cells. For this purpose, we studied the changes in MMP expression and activity due to AdCLU compared to AdMT in serum-starved HTM cells. Matrix metalloproteinase-2 (MMP2), also called type IV collagenase and gelatinase A, is widely distributed in many tissues. Its proteolytic activity depends on the activation of zymogen (proMMP2) (Weinreb et al., 2020). First, we examined the MMP2 gene expression (Figure 6a) and protein levels (Figure 6b), which showed no significant difference between AdCLU and AdMT. However, we found significant reduction in the gene expression of the tissue inhibitors of metalloproteinases (TIMPs) TIMP1 ($p = 0.01$) and TIMP2 ($p = 0.03$) (Figure 6c). TIMP1 and TIMP2 can interact with pro-MMP2 and thereby inhibiting its activation (Weinreb et al., 2020). Following this, we performed gelatin zymography to analyze the effect of AdCLU on MMP activation, which showed a significant increase in the active form of MMP2 (62 kDa) (n = 3, $p = 0.02$) with no change in pro-MMP2 (72 kDa) in AdCLU compared to AdMT (Figure 6d,e). Though an increase in MMP1 was observed, it was not possible to decipher whether the increase was in pro- or active-form of MMP1 (Figure 6d). Various forms of MMP-9 were observed (~215 kDa
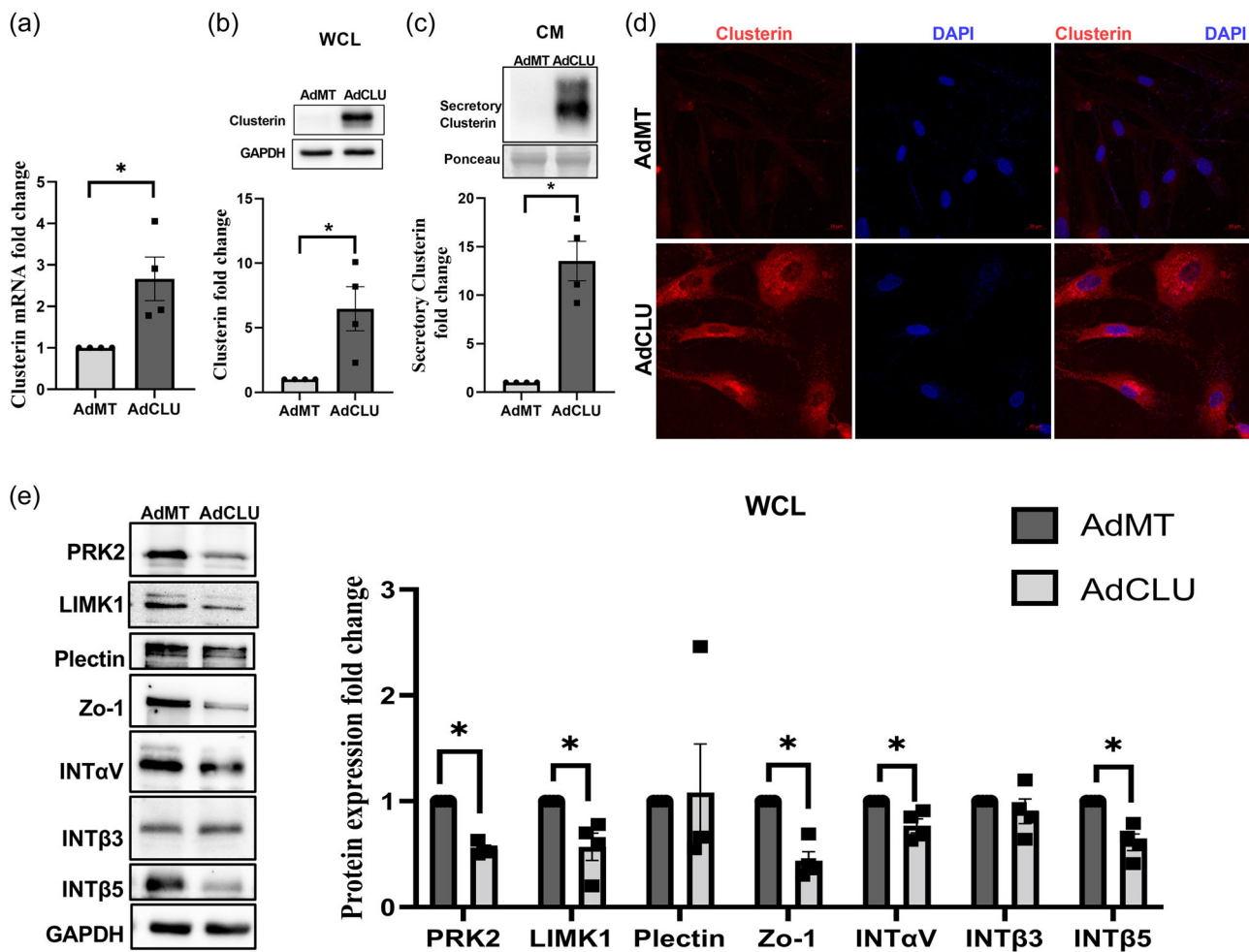
FIGURE 4 Effect of constitutive clusterin expression on TM actin cytoskeleton. Adenovirus-mediated constitutive expression of clusterin (AdCLU) in serum-starved HTM cells compared to control (AdMT) significantly increased - (a) clusterin mRNA expression, (b) clusterin protein levels in WCL, (c) in CM, and (d) cellular clusterin distribution (Alexa Flour 568/red) (bottom panel). GAPDH was used as a loading control for WCL, and Ponceau S-band at ~63 kDa was used for the CM. The nucleus was stained with DAPI in blue. Images were captured in z-stack in a confocal microscope, and stacks were orthogonally projected. Scale bar 20 microns. (e) Changes in the levels of actin cytoskeleton-associated proteins due to AdCLU. Western blot analysis showed significant decrease in the actin-associated proteins such as PRK2 and LIMK1, tight-junction protein Zo-1, membrane receptors- integrin- INTαV, INTβ5 in AdCLU compared to AdMT. GAPDH was used as a loading control for immunoblotting analysis. Values represent the mean ± SEM, where $n = 4$ (biological replicates). *$p ≤ 0.05$ was considered significant. CM, conditioned media; mRNA, messenger RNA; SEM, standard error of mean; TM, trabecular meshwork; WCL, whole-cell lysate

dimer, ~125 kDa complex, 92 kDa Pro- and 82 kDa active-MMP9) (Figure 6d) and there was a marginal decrease in the active-MMP-9 in AdCLU (data not shown). These results reveal MMP activation as mechanistic evidence for the negative regulation of ECM due to clusterin gain of function.

3.7 | Clusterin supplementation attenuates TGFβ2-induced fibrogenic process

We showed that the profibrotic TGFβ2 increased degradation of clusterin in the lysosomes. On the other hand, increase in secretory clusterin negatively regulated ECM and profibrogenic protein

expression in TM. To better understand if the secreted clusterin has any effect on TGFβ2-induced ECM accumulation and fibrosis, we utilized exogenous treatment of rhCLU on HTM cells. Serum-starved HTM cells were treated with rhCLU in the presence or the absence of TGFβ2. Treatment with TGFβ2 significantly induced COL1A ($n = 4$, $p = 0.02$) in the WCL but was significantly abrogated in the presence of rhCLU ($n = 4$, $p = 0.03$) (Figure 7a). Interestingly, though FN decreased with rhCLU treatment, the levels were not significant and similarly the increase due to TGFβ2 was not significant either (Figure 7a). In the CM, both COL1A and FN did not show changes compared to the control (Figure 7b).

On examining the profibrotic proteins, TSP-1 in WCL was significantly induced by TGFβ2 treatment ($n = 4$, $p = 0.02$)
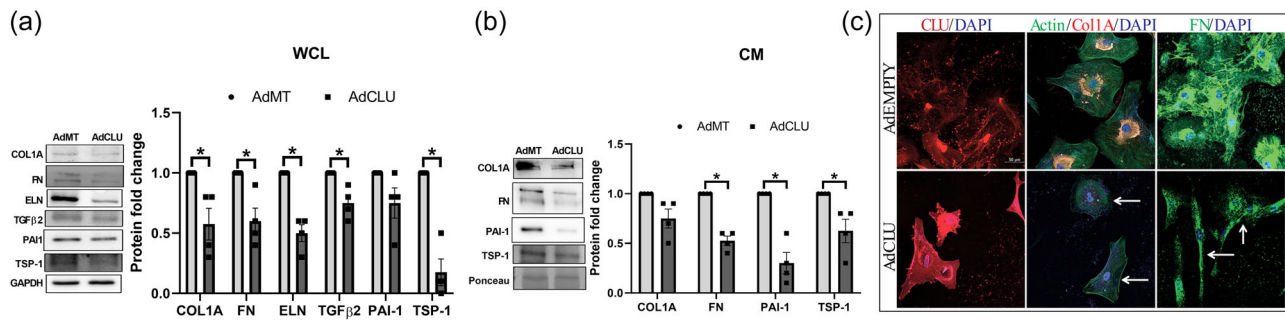
FIGURE 5 Effect of AdCLU on the levels and distribution ECM and pro-fibrotic proteins. Protein expression analysis by western blot showed significant decrease in - (a) ECM proteins-COL1A, FN, ELN, and pro-fibrotic TGFβ2 and TSP-1 in WCL, (b) secretory FN and pro-fibrotic PAI-1 and TSP-1 in CM showed - in AdCLU compared with AdMT. GAPDH was used as a loading control. Values represent the mean ± SEM, where n = 4 (biological replicates). *p ≤ 0.05 was considered significant. (d) Immunofluorescence imaging shows increase in clusterin distribution in AdCLU treatment (Alexa Flour 568/red) (first column in bottom panel) and a concomitant reduction in actin stress fiber distribution stained by phalloidin (green) (second column in bottom panel) compared to AdMT (top panel). AdCLU treatment reduced COL1A (Alexa Flour 568/red) (second column bottom panel), and FN (Alexa Flour 488/green) (third column bottom panel) distribution compared to AdMT. The nucleus was stained with DAPI in blue. Images were captured in z-stack in a confocal microscope, and stacks were orthogonally projected. Scale bar 50 microns. AdCLU, adenovirus-mediated constitutive expression of clusterin; ECM, extracellular matrix; DAPI, 4′,6-diamidino-2-phenylindole; SEM, standard error of mean; WCL, whole-cell lysate

(Figure 7c), which was annulled by rhCLU treatment (n = 4, p = 0.01). The profibrotic marker and a serine protease inhibitor, PAI-1 in WCL showed no significant changes (Figure 7c). In the CM, we found that TGFβ2 treatment significantly increased the secretion of PAI-1 (n = 4, p = 0.05), which was aborted by the addition of rhCLU (n = 4, p = 0.003) (Figure 7d). In the case of TSP-1 in CM, TGFβ2 significantly increased TSP-1 (n = 4, p = 0.04) secretion and the introduction of rhCLU significantly inhibited the secretion of TSP-1 (n = 4, p = 0.05) even in the presence of TGFβ2 (Figure 7d). Therefore, we demonstrate that clusterin possess an antifibrotic effect in TM and can reduce collagen increase due to pathological insult. Thus, suggesting that increasing clusterin levels can potentially lower pathological elevation in IOP.

4 | DISCUSSION

In this study, we have provided initial evidence and elucidated mechanistic insights into the role of the secretory chaperone protein, clusterin, in the regulation of actin cytoskeletal tension and ECM remodeling in TM.

Clusterin is a stress-related chaperone protein known to inhibit the precipitation of both intracellular and secreted proteins (Poon et al., 2000). Clusterin is expressed in the TM outflow pathway and is secreted into the AH. Interestingly, the secreted clusterin in AH appeared at different molecular weights compared to the TM clusterin found in the WCL and CM. Such differences in molecular weight can be attributed to the differential glycosylation patterns in clusterin and the composition of variedly glycosylated clusterin from different tissues in the anterior segments including the corneal endothelial cells, iris, ciliary body, and the lens. Clusterin glycosylation is important for its secretion and chaperone function (Itakura

et al., 2020; Prochnow et al., 2013; Rohne et al., 2014). It will be interesting to understand the role and degree of glycosylation in the functionality of clusterin in the TM outflow pathway. It will also be significant to elucidate if clusterin secreted from TM functions locally due to the specific glycosylation pattern and its "sticky" nature (Blaschuk et al., 1983). Furthermore, despite being a stress response protein, our findings provide evidence for compromised clusterin expression, glycosylation, and secretion due to different stressors on the TM known to cause ocular hypertension including CMS, which mimics the pulsatile stress due to cardiac cycle whereas the anterior segment perfusion cultures were at constant elevated pressure stress. We observed a decreasing trend (Figure 1e) in clusterin mRNA expression whereas a significant decrease in protein levels in the TM cells subjected to CMS. Changes in RNA expression analysis was done after 8 h of CMS, whereas the protein expression was performed after 24 h. This might have resulted in nonsignificant decrease in mRNA compared to a significant decrease in protein expression. A time-dependent study will be able to tease out the temporal clusterin mRNA and protein regulation under CMS. Here we identified that secretion of clusterin is hampered by TGFβ2 as it increased the lysosomal accumulation and degradation of clusterin, thereby providing the mechanistic link for loss of clusterin function in TGFβ2-mediated TM dysfunction. Decrease in clusterin levels has been linked to diseases of fibrosis where TGFβ is known to be elevated (Peix et al., 2018).

Interestingly, the downregulation of clusterin using siRNA – A) induced actin polymerization via induction of PRKD1, PRK2, and LIMK. PRKD1, a serine threonine kinase, localizes at the site of actin polymerization and stabilizes the actin by phosphorylating and inactivating the phosphatase SSH1/2/3 by binding to 14-3-3 (Eiseler et al., 2010). This stabilizes the formed actin. PRK2 is an effector of Rho family small GTPases, known to regulate actin-cytoskeleton
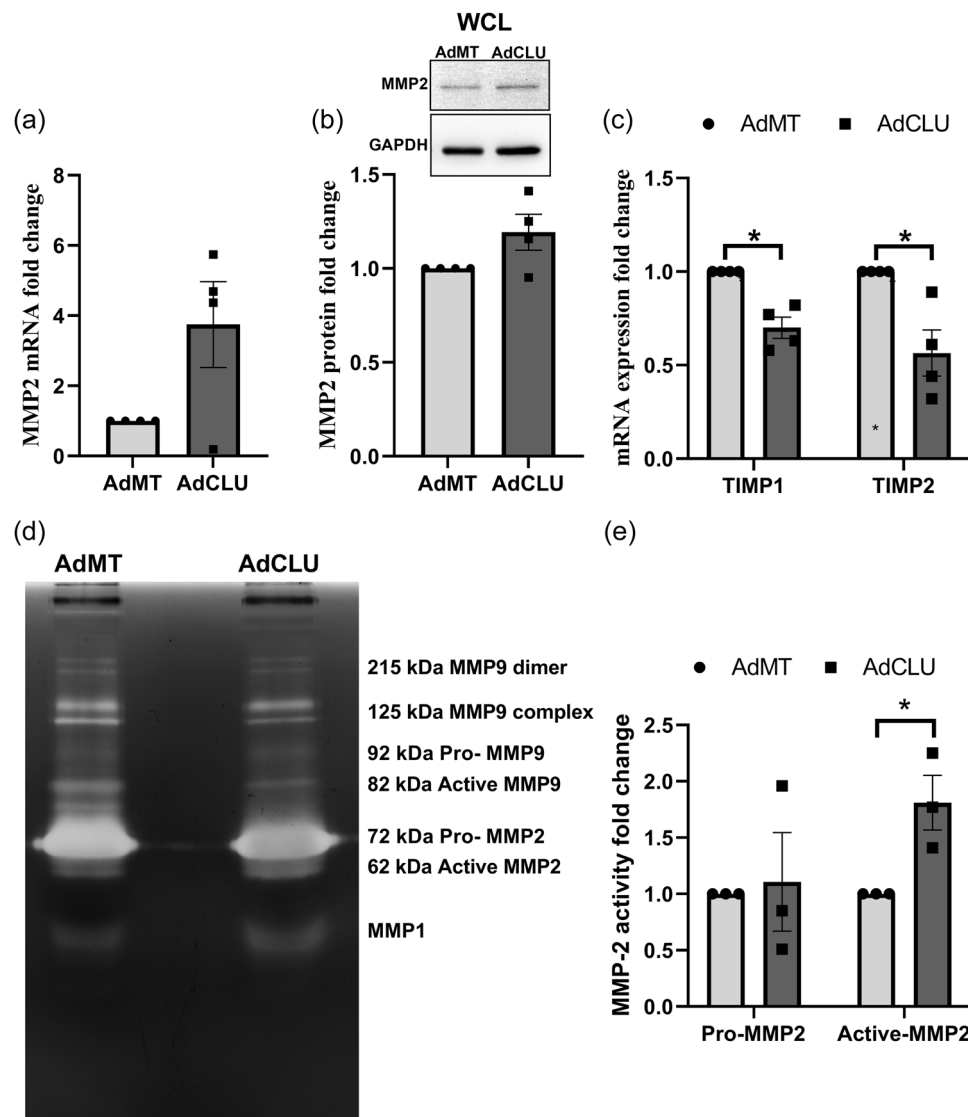
FIGURE 6 Clusterin regulates ECM remodeling by MMP activation. Serum-starved HTM cells transduced with AdCLU compared to AdMT shows – (a) no change in MMP2 mRNA expression, (b) no change on MMP2 protein expression. GAPDH was used as a loading control. (c) significant decrease in mRNA expression of tissue inhibitors of metalloproteinases (TIMP1 & TIMP2). (d) and (e) significant increase in active form of MMP2 (62 kDa) as visualized by gelatin zymography. No significant change is seen in pro-MMP2 (72 kDa). MMP1, and MMP-9 were detected. Values represent the mean ± SEM, where n = 3–4 (biological replicates). *p ≤ 0.05 was considered significant. AdCLU, adenovirus-mediated constitutive expression of clusterin; ECM, extracellular matrix; mRNA, messenger RNA; SEM, standard error of mean; WCL, whole-cell lysate

organization (Vincent & Settleman, 1997). Both PRKD1 and PRK2 converge on to LIM domain kinases (LIMKs), which are serine/threonine kinases promoting actin polymerization (Bernard, 2007; Eiseler et al., 2010; Vincent & Settleman, 1997); B) upregulated plectin-1, an actin linker and scaffolding protein is known to increase mechanical integrity and tissue stiffness (Inoue et al., 2010; Na et al., 2009), and C) increased the adhesome complexes including focal adhesion paxillin and its phosphorylation at Tyr 118 promoting contractile phenotype (Dumbauld et al., 2010; Pattabiraman et al., 2015a; Pavalko et al., 1995), and integrins including INTαV and INTβ5 potentially activating TGFβ signaling and inducing a fibrogenic response (Asano et al., 2005). The loss of clusterin function

in TM due to low levels of secreted clusterin induced changes in actin accompanied by the induction of vinculin and paxillin recruitment and the phosphorylation of paxillin suggesting an enhanced inside-out signaling towards integrin binding to ECM and recruitment of focal adhesion (Shen et al., 2012). In the TM outflow physiology, stimulus inducing the actin-based cytoskeletal contractility and perturbed ECM remodeling can elevate the IOP (Pattabiraman et al., 2015b; Soundararajan et al., 2021). Furthermore, this was confirmed when we used *Clu*^{−/−} mice, which does not make any clusterin and such complete lack of clusterin resulted in a significant IOP elevation within the first four months postbirth (~105 days). We believe that a cumulative increase in pressure and ocular hypertension over time
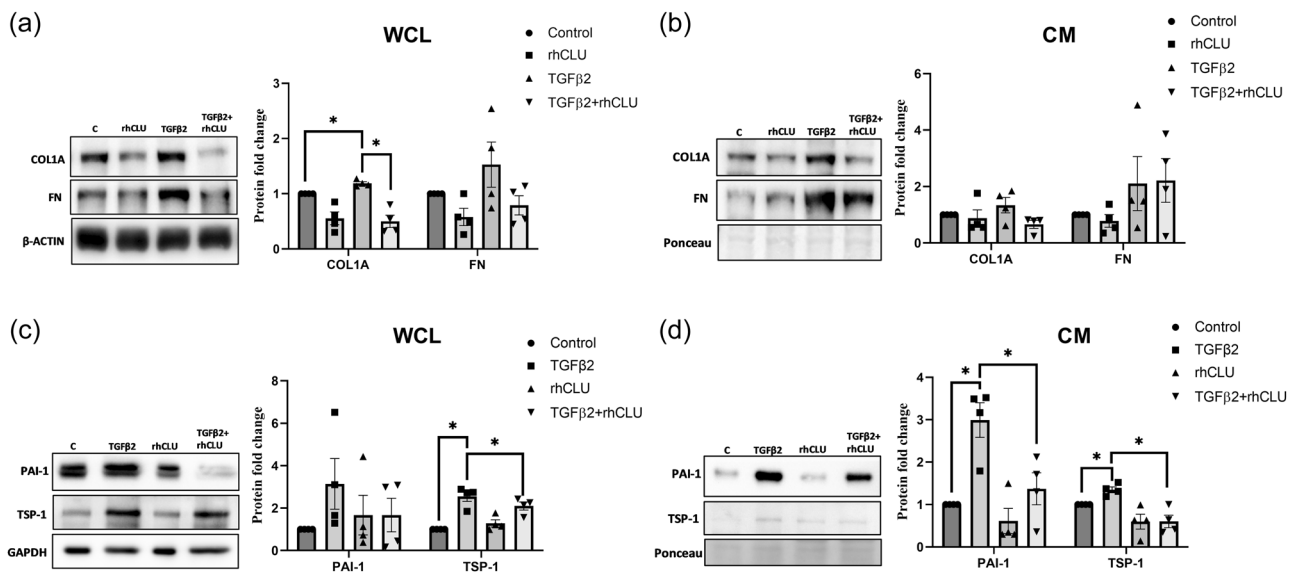
FIGURE 7 Clusterin supplementation attenuates TGFβ2-induced fibrogenic process. Serum-starved HTM cells treated with TGFβ2 exhibited significant increase in COL1A (WCL), TSP1 (WCL and CM), and PAI1 (CM) which was significantly suppressed by supplementation of rhCLU. β-actin or GAPDH was used as a loading control for WCL, and ponceau-S band was used as a loading control for CM. Values represent the mean ± SEM, where $n = 4$ (biological replicates). * $p \leq 0.05$ was considered significant. CM, conditioned media; SEM, standard error of mean; WCL, whole-cell lysate

would result in a glaucomatous phenotype in the clusterin null mice. Though we do not have a molecular understanding into such ocular hypertensive phenotype, additional characterization of the outflow pathway tissues in the $Clu^{-/-}$ mice should reveal greater details into the pathogenic process leading to elevated IOP and glaucoma if any. We hypothesize that when there is loss of clusterin, it increases actin polymerization and the adhesome complex recruitment including the focal adhesions and integrins increasing the internal force, which can induce recruitment of the ECM and/or alter ECM arrangement, thus lowering the outflow facility and increasing IOP (Faralli et al., 2019; Pattabiraman et al., 2015b).

On the contrary, the gain of function experiments using AdCLU revealed a significant decrease in PRK2 and LIMK1 inducing a loss of contractile machinery, integrins, and cell junction protein like Zo-1. LIMK inhibition aid in relieving systemic hypertension as well as elevated IOP-induced glaucoma (Harrison et al., 2009; Morales-Quinones et al., 2020). Such a decrease can potentiate the disengagement of ECM from the integrins and a decrease in ECM. This study established that AdCLU and supplementation of rhCLU decreased ECM and fibrotic process emphasizing the importance of clusterin in ECM remodeling. Concomitantly, decreasing cytoskeletal contractility, ECM, and lowering cell junction proteins including Zo-1 can increase the outflow facility and reduce the IOP (Cassidy et al., 2021; Faralli et al., 2019; Keller et al., 2009; Pattabiraman et al., 2015b; Vranka et al., 2015). We propose that the lowering of ECM is due to a significant downregulation of profibrotic proteins including TGFβ2, PAI-1, and TSP-1 and significantly increasing the MMP-2 activity (Pattabiraman et al., 2014; Pattabiraman et al., 2015b; Zhavoronkov et al., 2016). A recent study showed that heparan

sulfate (HS) acts as a receptor for clusterin binding and this clusterin-HS pathway helps in the clearance and degradation of aberrant extracellular proteins (Itakura et al., 2020). Such mechanism in the ECM clearance can be functional in TM, which needs to be better understood. Additional chaperone functions of clusterin includes: (a) clusterin can bind to and stabilizes cathepsin K (CTSK) (Novinec et al., 2012), which exhibits potent collagenolytic activity (Soundararajan et al., 2021) and (b) clusterin can aid in clearance of extracellular debris by receptor-mediated endocytosis (Bartl et al., 2001). It will be of significance to elucidate if gain of function of clusterin can increase the stability and activation of CTSK, thereby participating in the CTSK-mediated ECM degradation and clear the degraded ECM. Apart from HS, clusterin can also bind to other receptors such as TGFβR1, TGFβR2, VLDLR, LRP2, and LRP8 (Bartl et al., 2001; Peix et al., 2018). A deeper understanding of clusterin function mediated by receptor binding and signaling will help better understand its role in the regulation of actin in TM biology. Finally, though this study investigated the loss- and gain-of-function of clusterin on the TM, the physiological relevance of clusterin in the regulation of IOP will provide greater evidence into the role of clusterin in outflow physiology.

5 | CONCLUSION

In summary, we have shown that increased contractile force generation in TM due to loss of clusterin function elevates the IOP, and the gain of function by constitutively expressing secretory clusterin or supplementing with rhCLU lowers actin-based tension and attenuates profibrotic
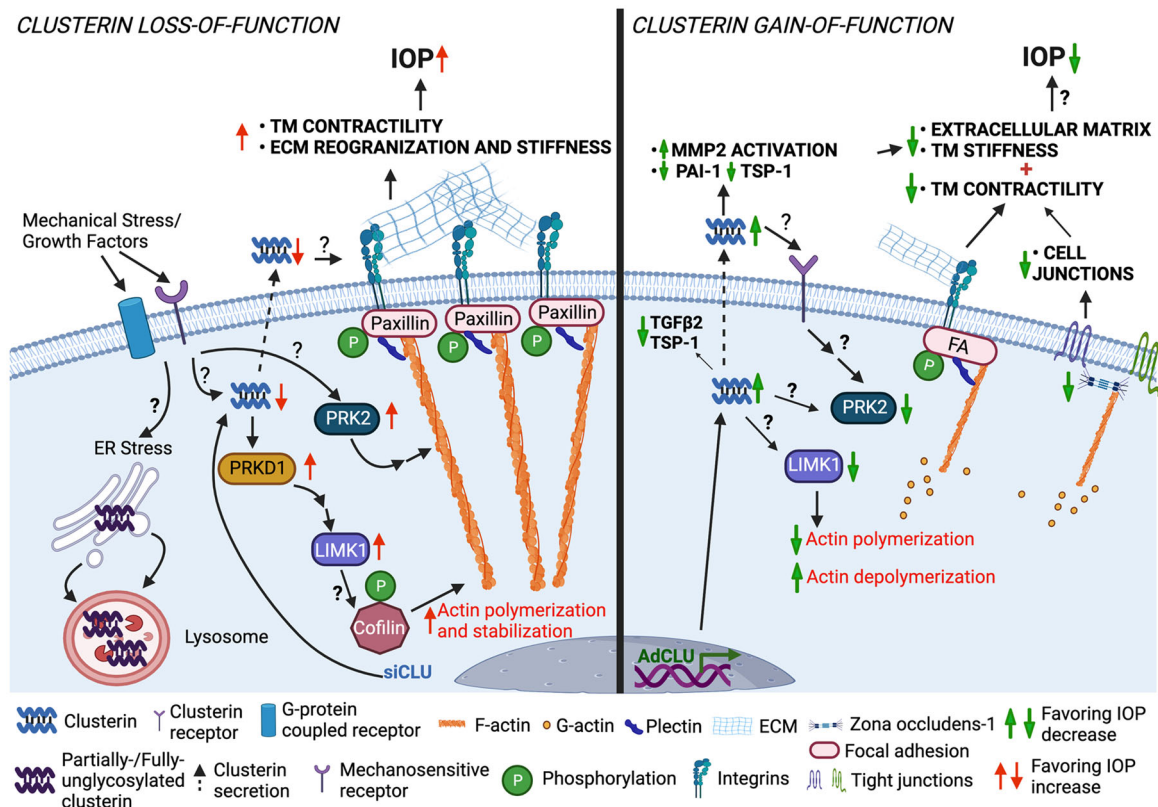
FIGURE 8 Proposed cellular and molecular mechanism of clusterin-mediated changes in actin contractile machinery and ECM-based TM tissue stiffness and IOP regulation (created with BioRender.com). We found that pathological insults that can cause IOP elevation, negatively influence clusterin expression and secretion in TM. Using loss-and gain-of-function studies in HTM cells in vitro, we identified that clusterin is an important cog in maintaining actin-based contractile machinery and ECM production, secretion, and fibrogenic function. Complete loss of clusterin significantly increased the IOP defining a functional role of clusterin in the aqueous humor outflow physiology and IOP regulation. ECM, extracellular matrix; IOP, intraocular pressure; TM, trabecular meshwork

ECM augmentation (Figure 8). Thus, demonstrating an important role of clusterin in the regulation of TM contractility and stiffness, and IOP regulation. However, the modality of receptor-mediated clusterin signaling to alter actin cytoskeleton, adhesome complexes, ECM binding to integrin, and chaperone function of clusterin in ECM clearance must be deciphered. The knowledge of the functional role of clusterin and the binding partners mediating ECM-cytoskeletal communication in TM will pave way for new therapeutic strategies to lower ocular hypertension.

AUTHOR CONTRIBUTIONS

ACKNOWLEDGMENTS

CONFLICTS OF INTEREST

The authors declare no conflicts of interest. The funders had no role in the design of the study; in the collection, analyses, or interpretation

of data; in the writing of the manuscript, or in the decision to publish the results.

INSTITUTIONAL REVIEW BOARD STATEMENT

Ethical review and approval were waived for the use of cadaveric human eyes for the isolation of the TM cells from human cadaveric corneal rims for this study.

REFERENCES

Aronow, B. J., Lund, S. D., Brown, T. L., Harmony, J. A., & Witte, D. P. (1993). Apolipoprotein J expression at fluid-tissue interfaces: Potential role in barrier cytoprotection. *Proceedings of the National Academy of Sciences of the United States of America*, 90(2), 725–729.

Asano, Y., Ihn, H., Yamane, K., Jinnin, M., Mimura, Y., & Tamaki, K. (2005). Involvement of alphavbeta5 integrin-mediated activation of latent transforming growth factor beta1 in autocrine transforming growth factor beta signaling in systemic sclerosis fibroblasts. *Arthtitis and Rheumatism*, 52(9), 2897–2905. https://doi.org/10.1002/art.21246

Bartl, M. M., Luckenbach, T., Bergner, O., Ullrich, O., & Koch-Brandt, C. (2001). Multiple receptors mediate apoJ-dependent clearance of cellular debris into nonprofessional phagocytes. *Experimental Cell Research*, 271(1), 130–141. https://doi.org/10.1006/excr.2001.5358

Bernard, O. (2007). Lim kinases, regulators of actin dynamics. *International Journal of Biochemistry and Cell Biology*, 39(6), 1071–1076. https://doi.org/10.1016/j.biocel.2006.11.011

Blaschuk, O., Burdzy, K., & Fritz, I. B. (1983). Purification and characterization of a cell-aggregating factor (clusterin), the major glycoprotein in ram rete testis fluid. *Journal of Biological Chemistry*, 258(12), 7714–7720.

Cassidy, P. S., Kelly, R. A., Reina-Torres, E., Sherwood, J. M., Humphries, M. M., Kiang, A. S., Farrar, G. J., O'Brien, C., Campbell, M., Stamer, W. D., Overby, D. R., Humphries, P., & O'Callaghan, J. (2021). siRNA targeting Schlemm's canal endothelial tight junctions enhances outflow facility and reduces IOP in a steroid-induced OHT rodent model. *Molecular Therapy. Methods & Clinical Development*, 20, 86–94. https://doi.org/10.1016/j.omtm.2020.10.022

Dabbs, R. A., & Wilson, M. R. (2014). Expression and purification of chaperone-active recombinant clusterin. *PLoS One*, 9(1), e86989. https://doi.org/10.1371/journal.pone.0086989

Diskin, S., Kumar, J., Cao, Z., Schuman, J. S., Gilmartin, T., Head, S. R., & Panjwani, N. (2006). Detection of differentially expressed glycogenes in trabecular meshwork of eyes with primary open-angle glaucoma. *Investigative Ophthalmology and Visual Science*, 47(4), 1491–1499. https://doi.org/10.1167/iovs.05-0736

Doudevski, I., Rostagno, A., Cowman, M., Liebmann, J., Ritch, R., & Ghiso, J. (2014). Clusterin and complement activation in exfoliation glaucoma. *Investigative Ophthalmology and Visual Science*, 55(4), 2491–2499. https://doi.org/10.1167/iovs.13-12941

Dumbauld, D. W., Shin, H., Gallant, N. D., Michael, K. E., Radhakrishna, H., & García, A. J. (2010). Contractility modulates cell adhesion strengthening through focal adhesion kinase and assembly of vinculin-containing focal adhesions. *Journal of Cellular Physiology*, 223(3), 746–756. https://doi.org/10.1002/jcp.22084

Eiseler, T., Hausser, A., De Kimpe, L., Van Lint, J., & Pfizenmaier, K. (2010). Protein kinase D controls actin polymerization and cell motility through phosphorylation of cortactin. *Journal of Biological Chemistry*, 285(24), 18672–18683. https://doi.org/10.1074/jbc.M109.093880

Faralli, J. A., Filla, M. S., & Peters, D. M. (2019). Role of fibronectin in primary open angle glaucoma. *Cells*, 8(12), https://doi.org/10.3390/cells8121518

Goel, M., Picciani, R. G., Lee, R. K., & Bhattacharya, S. K. (2010). Aqueous humor dynamics: A review. *The Open Ophthalmology Journal*, 4, 52–59. https://doi.org/10.2174/1874364101004010052

Harrison, B. A., Whitlock, N. A., Voronkov, M. V., Almstead, Z. Y., Gu, K. J., Mabon, R., Gardyan, M., Hamman, B. D., Allen, J., Gopinathan, S., McKnight, B., Crist, M., Zhang, Y., Liu, Y., Courtney, L. F., Key, B., Zhou, J., Patel, N., Yates, P. W., … Rawlins, D. B. (2009). Novel class of LIM-kinase 2 inhibitors for the treatment of ocular hypertension and associated glaucoma. *Journal of Medicinal Chemistry*, 52(21), 6515–6518. https://doi.org/10.1021/jm901226j

Inoue, T., Pecen, P., Maddala, R., Skiba, N. P., Pattabiraman, P. P., Epstein, D. L., & Rao, P. V. (2010). Characterization of cytoskeleton-enriched protein fraction of the trabecular meshwork and ciliary muscle cells. *Investigative Ophthalmology and Visual Science*, 51(12), 6461–6471. https://doi.org/10.1167/iovs.10-5318

Itakura, E., Chiba, M., Murata, T., & Matsuura, A. (2020). Heparan sulfate is a clearance receptor for aberrant extracellular proteins. *Journal of Cell Biology*, 219(3), https://doi.org/10.1083/jcb.201911126

Jeong, S., Ledee, D. R., Gordon, G. M., Itakura, T., Patel, N., Martin, A., & Fini, M. E. (2012). Interaction of clusterin and matrix metalloproteinase-9 and its implication for epithelial homeostasis and inflammation. *American Journal of Pathology*, 180(5), 2028–2039. https://doi.org/10.1016/j.ajpath.2012.01.025

Kasetti, R. B., Maddineni, P., Millar, J. C., Clark, A. F., & Zode, G. S. (2017). Increased synthesis and deposition of extracellular matrix proteins leads to endoplasmic reticulum stress in the trabecular meshwork. *Scientific Reports*, 7(1), 14951. https://doi.org/10.1038/s41598-017-14938-0

Kasetti, R. B., Maddineni, P., Patel, P. D., Searby, C., Sheffield, V. C., & Zode, G. S. (2018). Transforming growth factor β2 (TGFβ2) signaling plays a key role in glucocorticoid-induced ocular hypertension. *Journal of Biological Chemistry*, 293(25), 9854-9868. https://doi.org/10.1074/jbc.RA118.002540

Keller, K. E., Aga, M., Bradley, J. M., Kelley, M. J., & Acott, T. S. (2009). Extracellular matrix turnover and outflow resistance. *Experimental Eye Research*, 88(4), 676-682. https://doi.org/10.1016/j.exer.2008.11.023

Keller, K. E., Bhattacharya, S. K., Borrás, T., Brunner, T. M., Chansangpetch, S., Clark, A. F., Dismuke, W. M., Du, Y., Elliott, M. H., Ethier, C. R., Faralli, J. A., Freddo, T. F., Fuchshofer, R., Giovingo, M., Gong, H., Gonzalez, P., Huang, A., Johnstone, M. A., Kaufman, P. L., … Stamer, W. D. (2018). Consensus recommendations for trabecular meshwork cell isolation, characterization and culture. *Experimental Eye Research*, 171, 164–173. https://doi.org/10.1016/j.exer.2018.03.001

Kourtis, N., & Tavernarakis, N. (2011). Cellular stress response pathways and ageing: Intricate molecular relationships. *The EMBO Journal*, 30(13), 2520-2531. https://doi.org/10.1038/emboj.2011.162

Li, P., Shen, T. T., Johnstone, M., & Wang, R. K. (2013). Pulsatile motion of the trabecular meshwork in healthy human subjects quantified by phase-sensitive optical coherence tomography. *Biomedical Optics Express*, 4(10), 2051-2065. https://doi.org/10.1364/BOE.4.002051

Liton, P. B., Liu, X., Stamer, W. D., Challa, P., Epstein, D. L., & Gonzalez, P. (2005). Specific targeting of gene expression to a subset of human trabecular meshwork cells using the chitinase 3-like 1 promoter. *Investigative Ophthalmology and Visual Science*, 46(1), 183-190. https://doi.org/10.1167/iovs.04-0330

Liu, B., McNally, S., Kilpatrick, J. I., Jarvis, S. P., & O'Brien, C. J. (2018). Aging and ocular tissue stiffness in glaucoma. *Survey of Ophthalmology*, 63(1), 56-74. https://doi.org/10.1016/j.survophthal.2017.06.007

Luna, C., Li, G., Liton, P. B., Epstein, D. L., & Gonzalez, P. (2009). Alterations in gene expression induced by cyclic mechanical stress in trabecular meshwork cells. *Molecular Vision*, 15, 534-544.

Michel, D., Chatelain, G., North, S., & Brun, G. (1997). Stress-induced transcription of the clusterin/apoJ gene. *Biochemical Journal*, 328 (Pt 1), 45-50.

Morales-Quinones, M., Ramirez-Perez, F. I., Foote, C. A., Ghiarone, T., Ferreira-Santos, L., Bloksgaard, M., Martinez-Lemus, L. A. (2020). LIMK (LIM Kinase) inhibition prevents vasoconstriction- and hypertension-induced arterial stiffening and remodeling. *Hypertension*, 76(2), 393-403. https://doi.org/10.1161/hypertensionaha.120.15203

Na, S., Chowdhury, F., Tay, B., Ouyang, M., Gregor, M., Wang, Y., Wiche, G., Wang N. (2009). Plectin contributes to mechanical properties of living cells. *American Journal of Physiology Cell Physiology*, 296(4), C868-C877. https://doi.org/10.1152/ajpcell.00604.2008

Novinec, M., Lenarcic, B., & Baici, A. (2012). Clusterin is a specific stabilizer and liberator of extracellular cathepsin K. *FEBS Letters*, 586(7), 1062-1066. https://doi.org/10.1016/j.febslet.2012.03.004

Pattabiraman, P. P., Inoue, T., & Rao, P. V. (2015a). Elevated intraocular pressure induces Rho GTPase mediated contractile signaling in the trabecular meshwork. *Experimental Eye Research*, 136, 29-33. https://doi.org/10.1016/j.exer.2015.05.001

Pattabiraman, P. P., Maddala, R., & Rao, P. V. (2014). Regulation of plasticity and fibrogenic activity of trabecular meshwork cells by Rho GTPase signaling. *Journal of Cellular Physiology*, 229(7), 927-942. https://doi.org/10.1002/jcp.24524

Pattabiraman, P. P., Rinkoski, T., Poeschla, E., Proia, A., Challa, P., & Rao, P. V. (2015b). RhoA GTPase-induced ocular hypertension in a rodent model is associated with increased fibrogenic activity in the trabecular meshwork. *American Journal of Pathology*, 185(2), 496-512. https://doi.org/10.1016/j.ajpath.2014.10.023

Pattabiraman, P. P., & Toris, C. B. (2016). The exit strategy: Pharmacological modulation of extracellular matrix production and deposition for better aqueous humor drainage. *European Journal of Pharmacology*, 787, 32-42. https://doi.org/10.1016/j.ejphar.2016.04.048

Pavalko, F. M., Adam, L. P., Wu, M. F., Walker, T. L., & Gunst, S. J. (1995). Phosphorylation of dense-plaque proteins talin and paxillin during tracheal smooth muscle contraction. *American Journal of Physiology*, 268(3 Pt 1), C563-C571. https://doi.org/10.1152/ajpcell.1995.268.3.C563

Peix, L., Evans, I. C., Pearce, D. R., Simpson, J. K., Maher, T. M., & McAnulty, R. J. (2018). Diverse functions of clusterin promote and protect against the development of pulmonary fibrosis. *Scientific Reports*, 8(1), 1906. https://doi.org/10.1038/s41598-018-20316-1

Poon, S., Easterbrook-Smith, S. B., Rybchyn, M. S., Carver, J. A., & Wilson, M. R. (2000). Clusterin is an ATP-independent chaperone with very broad substrate specificity that stabilizes stressed proteins in a folding-competent state. *Biochemistry*, 39(51), 15953-15960.

Prochnow, H., Gollan, R., Rohne, P., Hassemer, M., Koch-Brandt, C., & Baiersdörfer, M. (2013). Non-secreted clusterin isoforms are translated in rare amounts from distinct human mRNA variants and do not affect Bax-mediated apoptosis or the NF-κB signaling pathway. *PLoS One*, 8(9), e75303. https://doi.org/10.1371/journal.pone.0075303

Quigley, H. A., & Broman, A. T. (2006). The number of people with glaucoma worldwide in 2010 and 2020. *British Journal of Ophthalmology*, 90(3), 262-267.

Rohne, P., Prochnow, H., Wolf, S., Renner, B., & Koch-Brandt, C. (2014). The chaperone activity of clusterin is dependent on glycosylation and redox environment. *Cellular Physiology and Biochemistry*, 34(5), 1626-1639. https://doi.org/10.1159/000366365

Shen, B., Delaney, M. K., & Du, X. (2012). Inside-out, outside-in, and inside-outside-in: G protein signaling in integrin-mediated cell adhesion, spreading, and retraction. *Current Opinion in Cell Biology*, 24(5), 600-606. https://doi.org/10.1016/j.ceb.2012.08.011

Soundararajan, A., Ghag, S. A., Vuda, S. S., Wang, T., & Pattabiraman, P. P. (2021). Cathepsin K regulates intraocular pressure by modulating extracellular matrix remodeling and actin-bundling in the trabecular meshwork outflow pathway. *Cells*, 10(11), 2864. https://doi.org/10.3390/cells10112864

Trougakos, I. P. (2013). The molecular chaperone apolipoprotein J/clusterin as a sensor of oxidative stress: Implications in therapeutic approaches: A mini-review. *Gerontology*, 59(6), 514-523. https://doi.org/10.1159/000351207

Urbich, C., Fritzenwanger, M., Zeiher, A. M., & Dimmeler, S. (2000). Laminar shear stress upregulates the complement-inhibitory protein clusterin: a novel potent defense mechanism against complement-induced endothelial cell activation. *Circulation*, 101(4), 352-355.

van Koolwijk, L. M., Ramdas, W. D., Ikram, M. K., Jansonius, N. M., Pasutto, F., Hysi, P. G., van Duijn, C. M. (2012). Common genetic determinants of intraocular pressure and primary open-angle glaucoma. *PLoS Genetics*, 8(5), e1002611. https://doi.org/10.1371/journal.pgen.1002611

Vincent, S., & Settleman, J. (1997). The PRK2 kinase is a potential effector target of both Rho and Rac GTPases and regulates actin cytoskeletal organization. *Molecular and Cellular Biology*, 17(4), 2247-2256. https://doi.org/10.1128/mcb.17.4.2247

Vranka, J. A., Kelley, M. J., Acott, T. S., & Keller, K. E. (2015). Extracellular matrix in the trabecular meshwork: Intraocular pressure regulation and dysregulation in glaucoma. *Experimental Eye Research*, 133, 112-125. https://doi.org/10.1016/j.exer.2014.07.014

Weinreb, R. N., Robinson, M. R., Dibas, M., & Stamer, W. D. (2020). Matrix metalloproteinases and glaucoma treatment. *Journal of Ocular Pharmacology and Therapeutics*, 36(4), 208-228. https://doi.org/10.1089/jop.2019.0146

Wyatt, A. R., Yerbury, J. J., Berghofer, P., Greguric, I., Katsifis, A., Dobson, C. M., & Wilson, M. R. (2011). Clusterin facilitates in vivo clearance of extracellular misfolded proteins. *Cellular and Molecular Life Science*, 68(23), 3919-3931. https://doi.org/10.1007/s00018-011-0684-8

Zhavoronkov, A., Izumchenko, E., Kanherkar, R. R., Teka, M., Cantor, C., Manaye, K., Sidransky, D., West M. D., Makarev E., Csoka A. B. (2016). Pro-fibrotic pathway activation in trabecular meshwork and lamina cribrosa is the main driving force of glaucoma. *Cell Cycle*, 15(12), 1643-1652. https://doi.org/10.1080/15384101.2016.1170261

SUPPORTING INFORMATION

Additional supporting information can be found online in the Supporting Information section at the end of this article.